

Local- and Large-Scale Drivers of Variability in the Coastal Freshwater Budget of the Western Antarctic Peninsula

**Key Points:**

- A novel 7-year series of seawater isotopes from the Antarctic Peninsula is used to trace freshwater inputs from different sources
- Variability in wind forcing and precipitation drive strong seasonal and interannual changes in observed sea ice melt and meteoric water
- Spatial scales of the key processes vary greatly, including the intermittent creation and destruction of very localized freshwater layers

Correspondence to:

M. P. Meredith,
mmm@bas.ac.uk

Citation:

Meredith, M. P., Stammerjohn, S. E., Ducklow, H. W., Leng, M. J., Arrowsmith, C., Brearley, J. A., et al. (2021). Local- and large-scale drivers of variability in the coastal freshwater budget of the Western Antarctic Peninsula. *Journal of Geophysical Research: Oceans*, 126, e2021JC017172. <https://doi.org/10.1029/2021JC017172>

Received 13 JAN 2021
Accepted 10 MAY 2021

Michael P. Meredith¹ , Sharon E. Stammerjohn² , Hugh W. Ducklow³ ,
Melanie J. Leng⁴ , Carol Arrowsmith⁴, J. Alexander Brearley¹ , Hugh J. Venables¹,
Mark Barham¹ , Jan Melchior van Wessem⁵ , Oscar Schofield⁶ , and Nicole Waite⁶ 

¹British Antarctic Survey, Cambridge, UK, ²Institute of Arctic and Alpine Research, University of Colorado, Boulder, CO, USA, ³Lamont-Doherty Earth Observatory, Columbia University, New York, NY, USA, ⁴National Environmental Isotope Facility, British Geological Survey, United Kingdom and School of Biosciences, University of Nottingham, Nottingham, UK, ⁵Institute for Marine and Atmospheric Research, Utrecht, The Netherlands, ⁶Rutgers University, Center of Ocean Observing Leadership, School of Environmental and Biological Sciences, Rutgers University, New Brunswick, NJ, USA

Abstract The west Antarctic Peninsula (WAP) is a region of marked climatic variability, exhibiting strong changes in sea ice extent, retreat of most of its glaciers, and shifts in the amount and form of precipitation. These changes can have significant impacts on the oceanic freshwater budget and marine biogeochemical processes; it is thus important to ascertain the relative balance of the drivers and the spatial scales over which they operate. We present a novel 7-year summer-season (October to March; 2011 to 2018) series of oxygen isotopes in seawater ($\delta^{18}\text{O}$), augmented with some winter sampling, collected adjacent to Anvers Island at the WAP. These data are used to attribute oceanic freshwater changes to sea ice and meteoric sources, and to deduce information on the spatial scales over which the changes are driven. Sea ice melt shows significant seasonality ($\sim 9\%$ range) and marked interannual changes, with pronounced maxima in seasons 2013/14 and 2016/17. Both of these extrema are driven by anomalous winds, but reflect strongly contrasting dynamic and thermodynamic sea ice responses. Meteoric water also shows seasonality ($\sim 7\%$ range) with interannual variability reflecting changes in the input of accumulated precipitation and glacial melt to the ocean. Unlike sea ice melt, meteoric water extremes are especially pronounced in thin (< 10 m) surface layers close to the proximate glacier, associated with enhanced ocean stratification. Isotopic tracers help to deconvolve the complex spatio-temporal scales inherent in the coastal freshwater budget, and hence improve our knowledge of the separate and cumulative physical and ecological impacts.

Plain Language Summary The Antarctic Peninsula shows very strong changes in climate, with long periods of warming interrupted by spells of cooling. At the same time, there have been large long-term and year-to-year changes in the sea ice cover west of the Peninsula, as well as in the speed of the melt and retreat of glaciers, and in the amount of snow that falls there. Upon melting, these freshwater sources affect the marine ecosystem in distinct ways, by injecting freshwater at different depths and supplying different nutrients, making it imperative to distinguish changes in these sources. Here, we use a new 7-year sequence of seawater measurements to calculate the amount of sea ice that melts into the ocean separately from the amount of snowmelt and glacier melt. We find very large changes in these sources, both on month-to-month and year-to-year timescales, and we identify causes of these changes. We find that some changes are driven by large-scale wind and precipitation variability, whereas other changes are caused much more locally. These findings are relevant to the marine life west of the Peninsula, and how it will respond to future climate change.

1. Introduction

The west Antarctic Peninsula (WAP; Figure 1) is a region characterized by pronounced climatic variability. Its atmosphere has warmed rapidly since the middle of the last century with significant periods of cooling superposed (Smith et al., 1996; Turner et al., 2016; Vaughan et al., 2003). These changes sit within a broader pattern of warming over many parts of West Antarctica over the past 30–50 years, with little overall change

© 2021. The Authors.

This is an open access article under the terms of the [Creative Commons Attribution License](https://creativecommons.org/licenses/by/4.0/), which permits use, distribution and reproduction in any medium, provided the original work is properly cited.

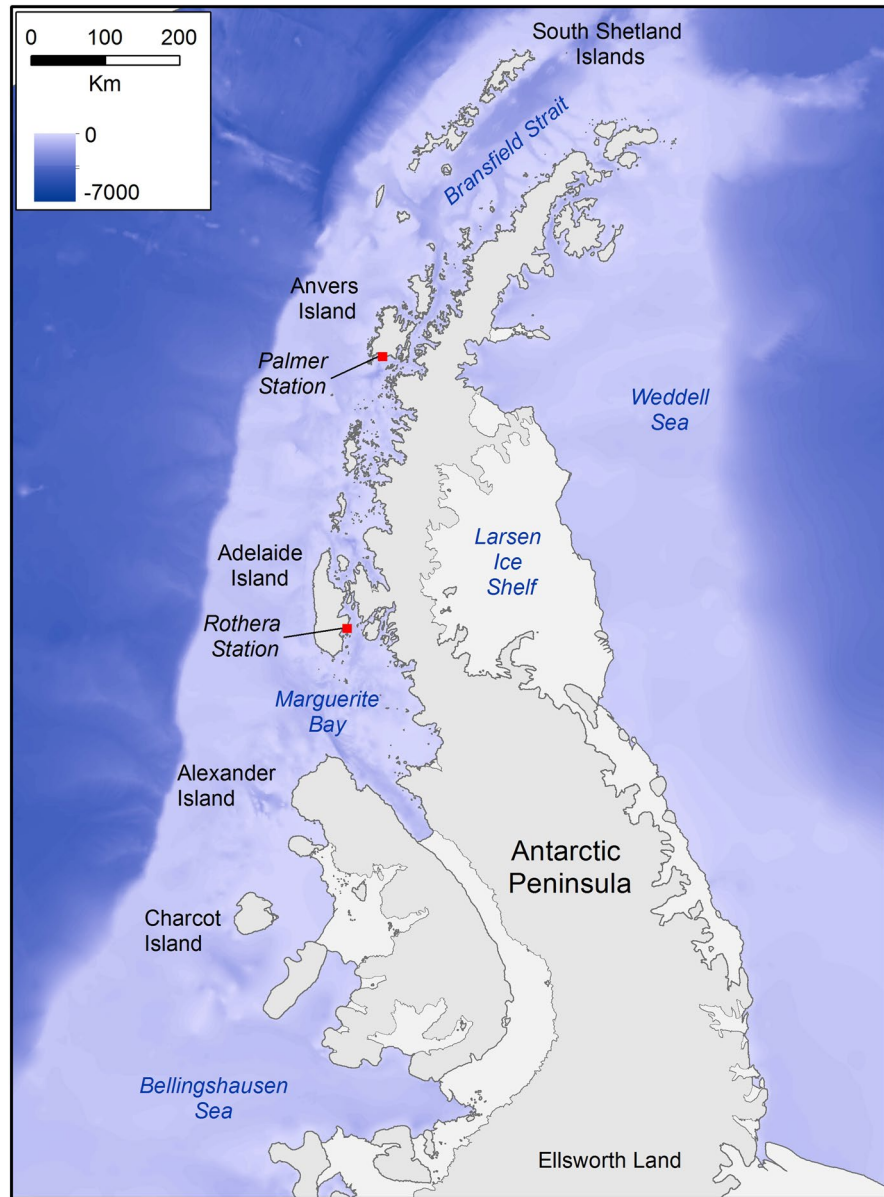


Figure 1. Bathymetry of the Antarctic Peninsula shelf and environs. Specific locations are marked, including Palmer Station at Anvers Island.

over East Antarctica (Meredith et al., 2019). The full reasons for the particular climatic sensitivity of the WAP are not yet fully established, though factors such as teleconnections with tropical regions are known to be important (e.g., Li et al., 2014).

Sea ice at the WAP is intimately coupled with the local climate (King, 1994; Meredith & King, 2005). This has an especially pronounced influence on atmospheric temperatures, since mean winds here have a marked onshore component so that air masses cross sea ice before reaching land (Harangozo, 2006; Smith & Stammerjohn, 2001; Turner et al., 2013). The ocean adjacent to the WAP exhibited a rapid loss of sea ice in the decades subsequent to the advent of satellite monitoring (Stammerjohn et al., 2003, 2008), consisting of a pronounced trend toward a later advance of sea ice in autumn, combined with a more moderate trend toward an earlier retreat in spring. More recently, total sea ice extent around Antarctica has shown pronounced extrema compared with the full length of the satellite records, with successive record highs in zonally-averaged sea ice extent during 2012–2014 followed by several years of record lows during 2016–2019

(Parkinson, 2019; Reid et al., 2020). At the WAP, winter sea ice extent and concentration showed moderate increases over the period since the turn of the century (Turner et al., 2016). This contrasts with the annual ice season duration, which showed marked increases in yearly variability post-2000, and which was punctuated by anomalously short annual ice seasons during 2007–2010, followed by anomalously long annual ice seasons during 2013–2016 (Henley et al., 2019). However, a marked retreat of sea ice to the west of the Peninsula and across the northern Weddell Sea was observed in spring 2016, coincident with an unprecedented circumpolar retreat of sea ice (Parkinson, 2019; Turner et al., 2016). Through 2019 and mid-way into 2020, circumpolar sea ice extent, including at the WAP, remained below the long-term mean, particularly during the summer-autumn period (Reid et al., 2020).

The multi-decade warming and climatic variability at the WAP has been concurrent with many other changes in the different components of its freshwater system. Atmospheric warming has been implicated as potentially important in glacial ice loss at the WAP, which is the main region in Antarctica with temperatures sufficiently high that significant surface melt and runoff may occur (Vaughan et al., 2003). The decadal increase in melt season duration at the WAP is consistent with the observed progression of ice shelf collapses (Scambos et al., 2000; van den Broeke, 2005), and while the majority of meltwater that percolates downwards will refreeze in the firn layer, there remains the possibility of significant runoff to the ocean (Barrand et al., 2013). Notwithstanding this, the observation that the majority of glaciers at the WAP are in retreat, with retreat rates accelerating (Cook et al., 2005; Pritchard & Vaughan, 2007), has more recently been ascribed to the influence of the heat from deep ocean waters. This is supplied in the form of warm Circumpolar Deep Water (CDW) from the Antarctic Circumpolar Current (ACC) penetrating onto and across the shelf to the WAP coastal regions, especially via deep glacially scoured canyons (Martinson & McKee, 2012; Venables et al., 2017). There is marked spatial variability in this process along the length of the WAP, resulting in marked latitudinal differences in retreat rates (Cook et al., 2016).

Precipitation at the WAP has increased in recent decades, with measurements from research stations indicating more precipitation events and a strengthening tendency for precipitation to fall as rain instead of snow (Kirchgäßner, 2011). A doubling of precipitation has been inferred for some WAP locations, using records from shallow ice cores (Thomas et al., 2008). Accumulation of snow on sea ice and its subsequent melt will contribute to the seasonal meteoric water budget at the WAP, although changes in snow accumulation on sea ice are currently not well constrained.

Each of these changes can exert profound influence on the physical, biogeochemical, and ecological functioning of the ocean. Freshwater injected at the ocean surface can create stably stratified layers, and hence can create environments more favorable for phytoplankton blooms (Mitchell & Holm-Hansen, 1991; Montes-Hugo et al., 2009; Saba et al., 2014; Venables et al., 2013; Vernet et al., 2008). Conversely, the destruction of stratification (e.g., by sea ice production) can have the opposite effect. The impacts of changes in stratification on phytoplankton dynamics can have consequences for the regional oceanic uptake of CO₂. Solid-phase sea ice is mobile under the influences of wind forcing and advection by ocean currents, the spatial variability of which can lead to complexity in the distributions and impacts of sea ice melt. It also constitutes an important habitat for a range of species from across trophic levels, and thus changes in sea ice have the potential to induce pronounced ecosystem changes adjacent to Antarctica (Meredith et al., 2019; Thomas & Dieckmann, 2002).

Glacial discharge to the ocean also has distinct impacts on regional physical oceanography, marine biogeochemistry, and the ecosystem. While low levels of micronutrients, such as iron, tend to limit primary production across much of the open Southern Ocean, its supply in coastal waters relieves this limitation and can lead to intense and extensive plankton blooms. Shallow sediments in the coastal zone can be influential in this supply, as can glaciers that scour underlying rock and sediments prior to supplying freshwater to the coastal seas (Annett et al., 2017; Boyd & Ellwood, 2010; Raiswell, 2011; Sherrell et al., 2018). Stronger glacial discharge to the ocean has the potential to deliver increased micronutrients (Hawkings et al., 2014), and could impact phytoplankton assemblage composition and biomass (Moline et al., 2004; Sherman et al., 2020). For example, Dierssen et al. (2002) noted that >70% of the phytoplankton blooms observed offshore of Anvers Island (Figure 1) occurred soon after meltwater pulses from local glaciers.

The depth at which glacial melt enters the ocean has the potential to be a key factor in its physical and ecological impact. Shallow injection from surface runoff or near-surface glacial melt will tend to increase stratification, and will supply any micronutrients or other biologically-active substances carried by the meltwater directly into the euphotic zone (Meredith et al., 2018). Conversely, glacial melt that occurs at depth due to melting by warm deep waters (or surface runoff that has percolated down to the glacier bed before reaching the ocean) will typically result in rising buoyant plumes that ascend until they reach a level of neutral buoyancy, which can be close to the surface or below the euphotic zone (Cape et al., 2019).

A further variant of the impact of glacial discharge is via the calving/drift of icebergs, and while the WAP is not typically influenced by large icebergs, it is impinged upon by a significant number of smaller ones (Tournadre et al., 2016). These icebergs can affect primary production by modifying the freshwater distribution and water column stability, and the ocean's geochemical properties (Duprat et al., 2016). They can also impact benthic ecosystems destructively by scouring when their keels extend to the seabed (Smale et al., 2008).

Climatic change at the WAP continues, and recently there have been observations of 32-year record-high surface melt rates at George VI Ice Shelf, concurrent with atmospheric temperatures over 20°C at the northern WAP that have been dubbed an Antarctic heatwave (Banwell et al., 2020). Given these extrema and their profound potential implications, combined with limited predictive skill concerning their future evolution, it is important that we improve our mechanistic understanding of the WAP system and its response to climate change.

In this study, we use a novel 7-year (2011–2018) series of freshwater tracer data from a coastal WAP site to quantify and attribute the changes in the freshwater input to the ocean, with a particular emphasis on deconvolving locally-driven changes and those driven on regional and larger scales. By doing so, we derive new information on how the WAP freshwater system has changed in recent years (including a period of rapid change in some of the key freshwater elements), and generate refined mechanistic understanding that will help improve knowledge of how it may change in future as climate change progresses.

2. Data Sources and Methods

2.1. Sample Acquisition and Processing

Water samples were collected quasi-weekly during summer (typically, from late October to March) from two sites near Palmer Research Station at Anvers Island at the WAP (Figure 2). The sampling sites, Palmer Stations B and E (Figure 2), are within the boating limits at Palmer Station. Station B (64.7795°S; 64.0725°W) is less than 1 km from the nearest point on Anvers Island, and a short trip from Palmer Station. This location affords consistent access in light to moderate sea ice cover. Station B is protected by islands to the north, east, and west, but exposed to the open Bellingshausen Sea to the south. Station E (64.815°S; 64.0405°W) is close to the limit of permitting boating operations, and exposed to the continental shelf and open sea. Stations B and E are in water 75 and 200 m deep, respectively. The start of the sampling season, constrained mainly by sea ice preventing boat access, ranges from mid-October to late December. During winter, boat sampling is not conducted; instead, a program of sampling at Palmer Station's seawater inlet (SWI: 64.7738°S; 64.0545°W) was initiated. The intake for this system is at 5.8 m depth. The sampling sites reside at different levels of proximity to the shallow marine-terminating Marr Ice Piedmont and fringing land-based ice masses, including some on the smaller adjacent islands (Figure 2). Typical water depths adjacent to the Marr Ice Piedmont are just a few tens of meters, with a deeper channel running past Palmer Station and Station B to the more open shelf.

Water samples were obtained from these sites using Niskin bottles deployed from a rigid inflatable boat, and closed either at the surface or 10 m depth. From the Niskin bottles, samples were drawn into 50 ml glass vials, which were sealed with stoppers and aluminum crimps. These samples were transported by dark cool stow to the UK's National Environmental Isotope Facility at the British Geological Survey. They were then analyzed for their oxygen isotope composition ($\delta^{18}\text{O}$, the standardized ratio of ^{18}O to ^{16}O), using the CO_2 equilibration method with an Isoprime 100 mass spectrometer plus the Aquaprep device. Isotope measurements were calibrated against internal and international standards, including VSMOW2 and VSLAP2. Based on duplicate analysis, analytical reproducibility of around $\pm 0.02\text{‰}$ was obtained for these samples. Concurrent with

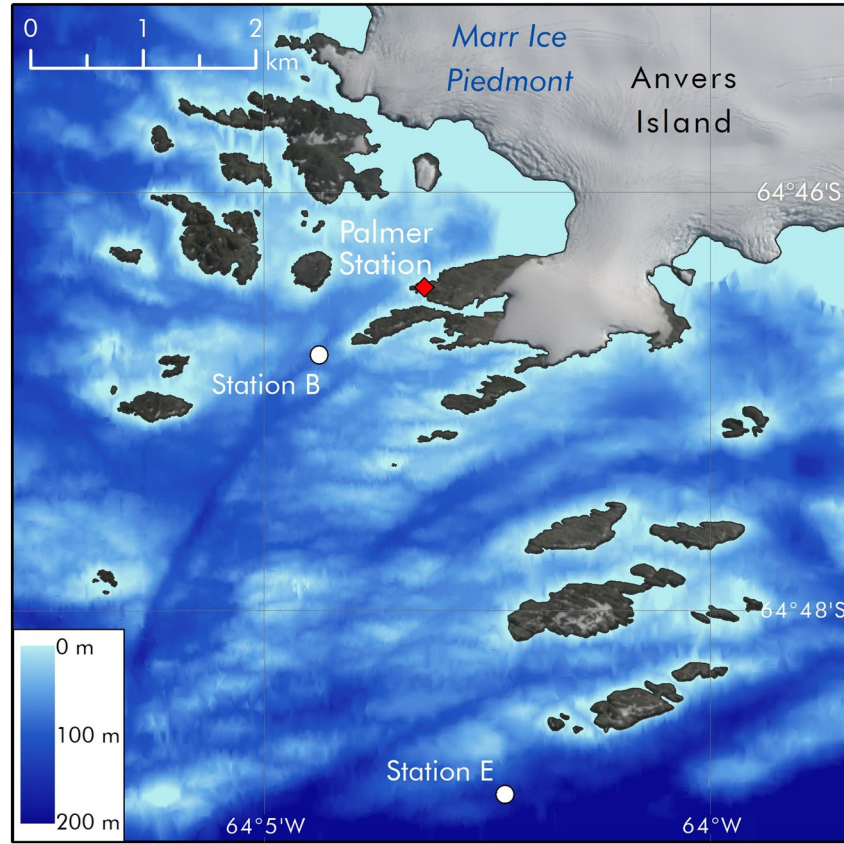


Figure 2. Immediate locality of Palmer Station, Anvers Island. The sites of sample collection (Stations B and E and Palmer Station) are marked.

the Station B and E sampling for $\delta^{18}\text{O}$, profiling of the water column was conducted using a SeaBird SBE19+ Conductivity Temperature Depth (CTD) profiler. From these casts, mixed layer depth (MLD) was derived using a criterion based on the vertical maximum of buoyancy, as per Carvalho et al. (2017). Ocean data used here are available at <https://portal.edirepository.org/nis/mapbrowse?packageid=knb-lter-pal.309.1>.

2.2. Mass Balance Calculations

Using the $\delta^{18}\text{O}$ and salinity data, we quantitatively separated sea ice melt from meteoric water (glacial melt and precipitation) by solving a simple 3-endmember mass balance. This was originally developed for the Arctic (Östlund & Hut, 1984), and was adapted for freshwater studies at the WAP by Meredith et al. (2008). It imposes an assumption that each water sample is comprised of three constituent components, namely sea ice melt, meteoric water, and CDW. At the WAP, this balance can be expressed as follows:

$$\begin{aligned} F_{\text{sim}} + F_{\text{met}} + F_{\text{cdw}} &= 1 \\ S_{\text{sim}} \cdot F_{\text{sim}} + S_{\text{met}} \cdot F_{\text{met}} + S_{\text{cdw}} \cdot F_{\text{cdw}} &= S \\ \delta_{\text{sim}} \cdot F_{\text{sim}} + \delta_{\text{met}} \cdot F_{\text{met}} + \delta_{\text{cdw}} \cdot F_{\text{cdw}} &= \delta \end{aligned} \quad (1)$$

where F_{sim} , F_{met} , and F_{cdw} are the fractions of sea ice melt, meteoric water, and CDW that are being solved for; S_{sim} , S_{met} , and S_{cdw} are the salinities of the pure endmembers of the respective constituent waters; δ_{sim} , δ_{met} , and δ_{cdw} are corresponding $\delta^{18}\text{O}$ values for these endmembers; and S and δ are the measured salinity and $\delta^{18}\text{O}$ of the water sample. Using this mass balance, negative values for sea ice melt are possible and are indicative of net sea ice production from the waters sampled, that is, a net salinification from brine rejection as opposed to a net freshening from sea ice melt.

Table 1
Endmember Values Used for Solving the Mass Balance Given in Equation 1

	Salinity	$\delta^{18}\text{O}$ (‰)
Sea ice melt	7	+1.1
Meteoric water	0.0	-12.0
Circumpolar Deep Water	34.65	0.0

This decomposition has been used successfully at the WAP previously, in Marguerite Bay (Figure 1) (Meredith et al., 2008, 2010), at King George Island in the South Shetlands (Meredith et al., 2018), and across the width of the shelf between Anvers Island and as far south as Charcot Island (Meredith et al., 2013, 2017). In each case, endmember values are chosen in order to reflect the local/regional freshwater and oceanic conditions as closely as possible. For the Palmer Station series, the endmembers chosen are given in Table 1.

The CDW endmember values were based on measurements collected close to Anvers Island, as per Meredith et al. (2017). The sea ice melt values are appropriate values for the WAP based on previously published analyses (Meredith et al., 2013, 2017). The mass balance (Equation 1) is most sensitive to the meteoric water endmember chosen; this is chosen here based on previous analyses and literature (Corbett et al., 2017; Meredith et al., 2013, 2017), and values from sampling in meltwater streams immediately adjacent to Palmer Station (Mike Brown; Rutgers University; pers. comm.). Sensitivity analyses have shown that this set of equations yields absolute freshwater concentrations with an accuracy better than 1%, and that the series produced are internally consistent such that temporal changes in freshwater concentrations are more precisely resolved (Meredith et al., 2008).

2.3. Palmer Station Meteorological Data

The meteorological instrumentation at Palmer Station is operated by the University of Wisconsin, and include sensors to measure air temperature, rainfall, snow precipitation, and snow depth. Full details and data are available at <https://portal.edirepository.org/nis/metadataviewer?packageid=knb-lter-pal.214.3>. Positive degree days (PDD) were calculated as the integral of positive surface air temperatures, starting on the 1st of August each year and extending to 31st of July of the following year. This comfortably encompasses the main period when surface air temperatures are persistently above zero: the PDD values remain low until the onset of spring, then rise rapidly before approaching an asymptote at their annual maximum in autumn/winter.

2.4. Regional Atmospheric Climate Model 2

We used simulated precipitation from version 2.3p2 of the Regional Atmospheric Climate Model 2 (RACMO2; van Wessem et al., 2018), which has been configured for use in glaciated regions. It was run with a horizontal resolution of 5.5 km, and with 40 vertical levels. It was forced at the boundaries using ERA-Interim reanalyses (Dee et al., 2011). Model output used here extended from 2011 to 2019, thus encompassing the period of in situ observations used. We demonstrated previously that this model provides a realistic depiction of the WAP meteoric water system, including its response to changes in coupled modes of climate variability (van Wessem et al., 2017).

2.5. Climate Data

Several sea ice products, ranging in resolution, are used to characterize regional changes in sea ice at the WAP. The coarsest resolution data comprise the monthly sea ice concentrations from Version 3.1 of the Goddard Space Flight Center (GSFC) Bootstrap Scanning Multi-channel Microwave Radiometer-Special Sensor Microwave/Imager (SMMR-SSM/I) time series (Comiso, 2000; Comiso & Nishio, 2008), here spanning 1979 to 2018 (40 years). These sea ice concentration data are gridded to 25 km and are provided by the EOS Distributed Active Archive Center (DAAC) at the National Snow and Ice Data Center (NSIDC, University of Colorado at Boulder, <https://nsidc.org/data/NSIDC-0051/versions/1>). The advantage of these coarser-resolution sea ice concentration data is that they comprise the longest time series available, and are used here to characterize monthly anomalies based on their 40-year means.

In contrast, higher-resolution sea ice concentration data are used to characterize finer-scale features of the sea ice cover on key days of interest. These daily sea ice concentrations are from the ARTIST Sea Ice (ASI)

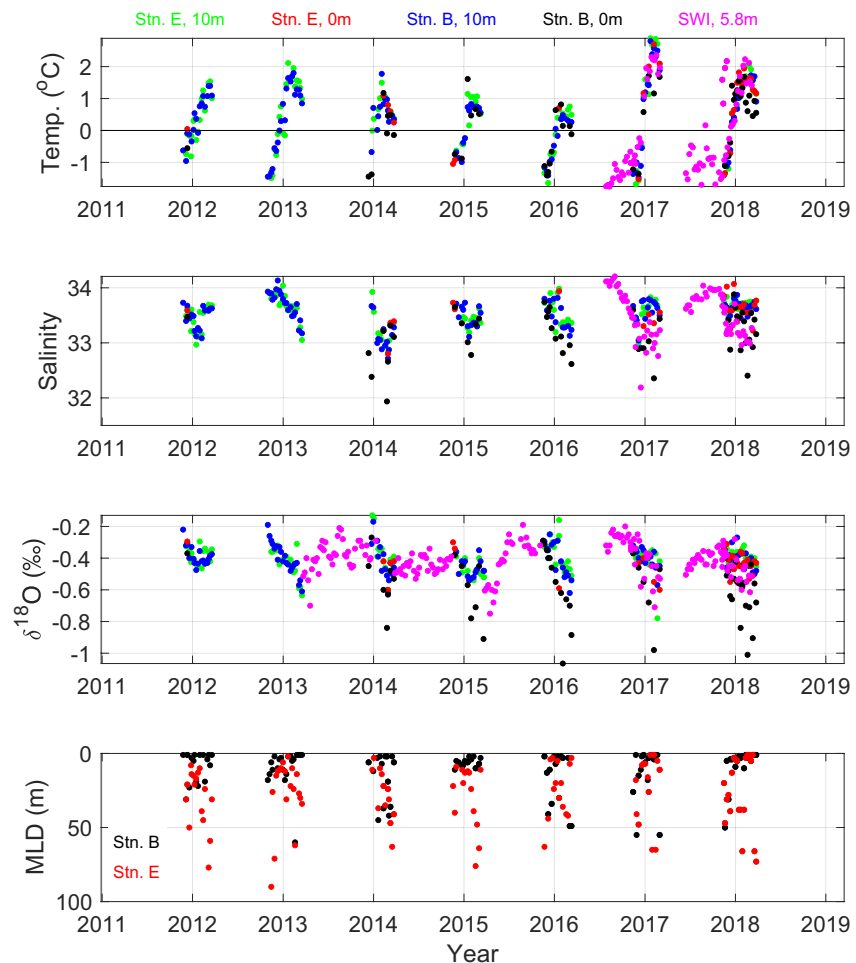


Figure 3. Upper panel: time series of ocean temperature at Palmer Station. Red and green symbols denote station E; black and blue symbols denote station B; magenta symbols denote seawater inlet (SWI) sampling at Palmer Station (Figure 2). Depths of sampling are as indicated. Second Panel: as for upper panel, but for salinity. Third Panel: as for upper panel, but for $\delta^{18}\text{O}$. Lower Panel: as for upper panel, but for Mixed Layer Depth (MLD).

algorithm version 5 (Spreen et al., 2008) using Advanced Microwave Scanning Radiometer 2 (AMSR2) data. These sea ice concentration data are gridded to 3.125 km and are available from the Universität Bremen (<https://www.seaice.uni-bremen.de>) for the period since 2012.

Monthly winds and weekly ice motion data are used to infer dynamical changes in the sea ice cover. The numerically-analyzed monthly 10-m height winds are from the European Centre for Medium Range Weather Forecasts (ECMWF) Interim Reanalysis (ERA-I) (Bracegirdle, 2013; Dee et al., 2011), from which we determined monthly wind anomalies based on their 40-year means. The weekly ice motion data are from the Polar Pathfinder 25 km EASE-Grid sea ice motion vectors, version 4. Derived ice motion vectors are based on a combination of satellite (AVHRR, AMSR, SMMR, SSMI/S) and buoy data using methods described by Tschudi et al. (2020), and are provided by the EOS DAAC at the NSIDC.

3. Temporal Changes in Oceanic Freshwater Balance at Palmer Station

3.1. Variability in Salinity and $\delta^{18}\text{O}$

While year-round ocean data from Palmer Station are not available for most of the period investigated here, clear seasonality and marked interannual variability are still discernible in each of the series produced (Figure 3). Temperature varies between the freezing point in winter and a maximum of 1°C–3°C in summer,

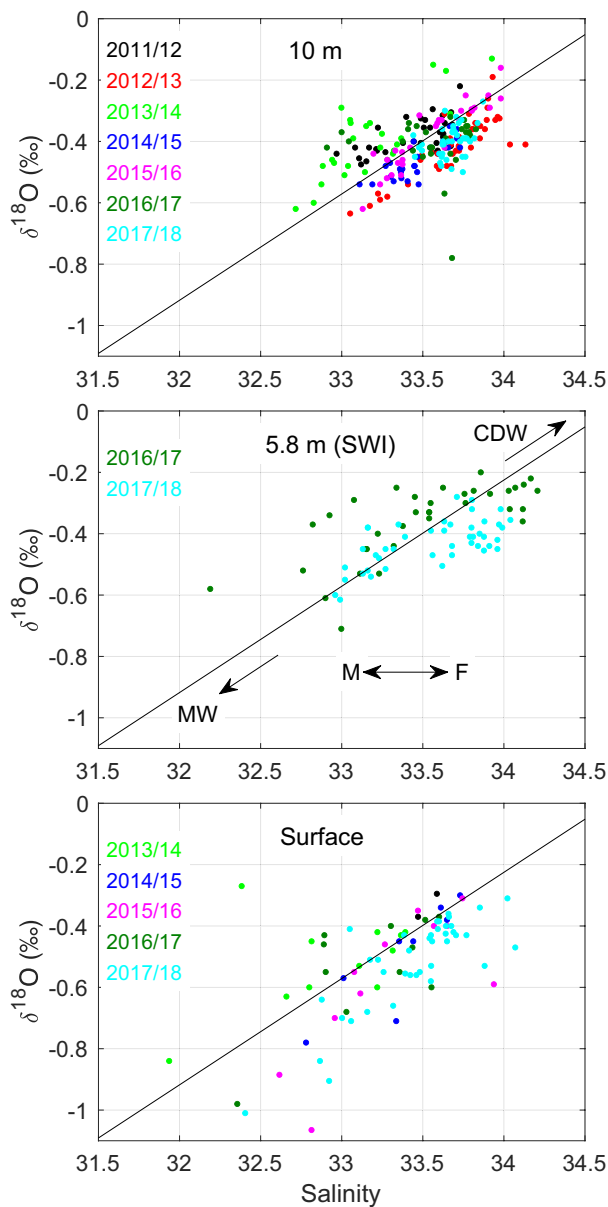


Figure 4. Data from the Palmer Station series (Figure 3) cast in salinity- $\delta^{18}\text{O}$ space. Panels are (top) 10 m sampling depth, (middle) 5.8 m sampling depth, (bottom) surface sampling. The diagonal line denotes the mixing line between ambient Circumpolar Deep Water (CDW) and Meteoric Water (MW): addition of MW would move the locus of points along this line toward fresher, isotopically-lower values, whereas addition of CDW would have the converse effect. The impact of sea ice melt (M) and freeze (F) is displayed; these processes would move the locus of points near-horizontally in the direction indicated. The sampling years are distinguished by color.

no corresponding points in the 10 m data. A small number of points are offset to the left of the meteoric water mixing line; these are due to different combinations of sea ice melt (toward the top of the figure) and meteoric water (toward the bottom), but each represent freshening of the ocean.

with summer seasons of 2015/16 and 2016/17 marking interannual cold and warm extremes, respectively. Salinity varies between around 33.0 and 34.0 on seasonal timescales, with some extreme fresh occurrences (down to 32.0) present during the summer months. $\delta^{18}\text{O}$ constitutes the most complete record amongst our data, since sample collection was enabled ahead of salinity and temperature logging from the SWI. The general seasonal cycle for $\delta^{18}\text{O}$ varies between around -0.6‰ and -0.2‰ , with sporadic isotopically-light instances in summer, yielding values as low as -1.0‰ . We have confidence that these instances are not errors in the data, since all spikes are duplicated and the data quality assured. The marked seasonality in $\delta^{18}\text{O}$ is an immediate indicator that the seasonality in salinity is not caused solely by sea ice processes. Typically, the freshest, isotopically-lightest waters are sampled toward the end of the summer sampling period (March/April), when accumulated freshwater inputs have reached their maxima and ahead of the onset of winter. MLD is typically shallower than 50 m, with some instances approaching 90 m. It is noteworthy that the fresh, isotopically-light extrema are predominantly at Site B and occur in the surface layer sampling, and that these coincide with the low values for MLD.

Further insight into the processes underlying the temporal changes in freshwater composition can be gained by considering the data in salinity- $\delta^{18}\text{O}$ space (Figure 4). Addition of meteoric water moves the locus of points diagonally downwards toward fresher, isotopically-lighter values, whereas mixing with saline ocean water has the opposite effect. Sea ice processes move the locus of points almost horizontally, with sea ice melt adding freshwater but having minimal effect on $\delta^{18}\text{O}$, and sea ice formation raising the salinity via brine rejection but again having minimal impact on $\delta^{18}\text{O}$.

Figure 4 reveals some pronounced differences between the years of sampling. Data from 2013/14 reside almost entirely to the left of the diagonal meteoric water mixing line, indicating a strong effect from net sea ice melt at that time. By contrast, other years are more neutral (2011/12; 2015/16) or have a tendency toward clustering to the right of the meteoric water mixing line, with 2017/18 being especially illustrative of the latter. It should be noted that within-year variability is incorporated into the locus of points, so that (for example) 2016/17 includes values on both sides of the mixing line due to temporal changes during the season of sampling.

Consistent with Figure 3, there are a number of extrema away from the meteoric water mixing line. Those that lie to the right of the line are predominantly from the surface sampling, and are indicative of stable stratification caused by the addition of meteoric water. (This may seem initially counter-intuitive, since the points lie away from the meteoric water mixing line, however, their location reflects both salinification by sea ice formation and freshening by the addition of meteoric water, with the latter process dominant.) As with the time series (Figure 3), we have confidence that these points are not errors in the data since there are virtually

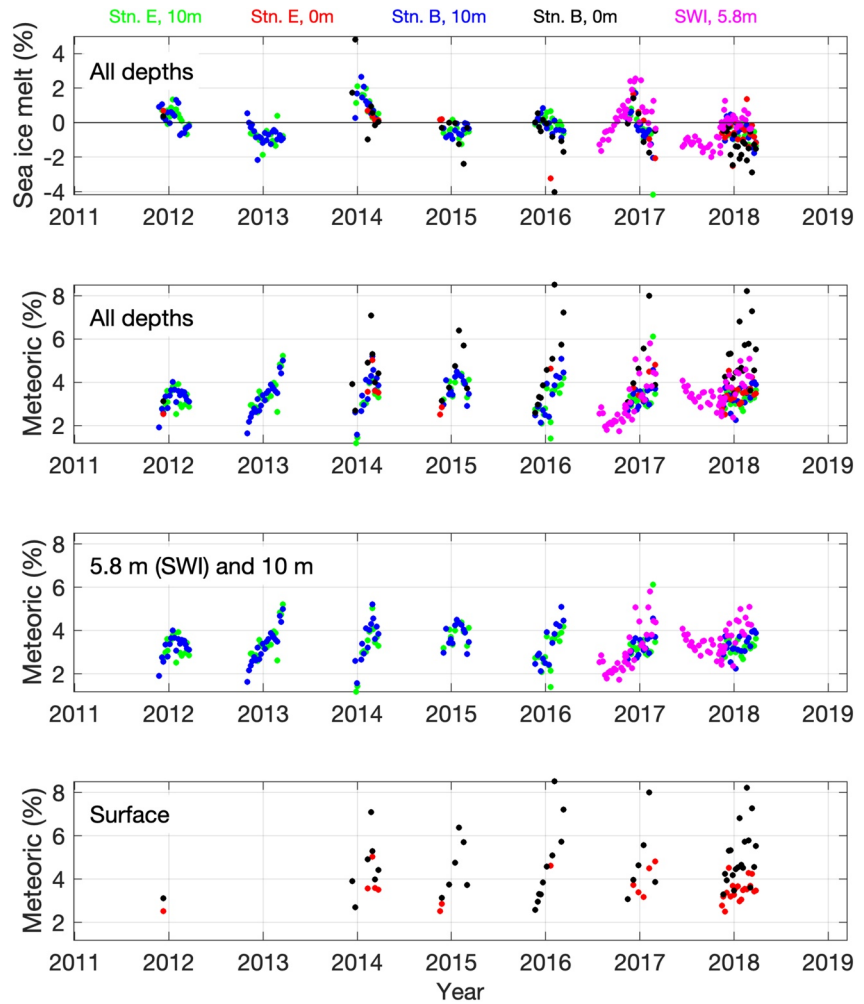


Figure 5. Series of sea ice melt (upper panel) and meteoric water (second panel) from the Palmer Station time series. To improve clarity, the third panel shows meteoric water from just 10 and 5.8 m (seawater inlet [SWI]), and the fourth panel shows meteoric water from just the surface sampling. Color convention is as per Figure 3.

3.2. Variability in Sea Ice Melt and Meteoric Water

Changes in the relative freshwater contents can be quantified using the mass balance derived from Equation 1. This shows that sea ice melt varies seasonally between around -2% and $+2\%$ in general (Figure 5), though full winter coverage is not available due to incomplete overlapping series of salinity and $\delta^{18}\text{O}$. There is distinct interannual variability in peak values superposed on the seasonality. The high seasonal values of F_{sim} in January/February 2014 are consistent with the general shelf-wide conditions at that time, as reflected in January 2014 cruise data that showed elevated values of sea ice melt across the continental shelf to the shelf break and beyond, compared with the previous three Januaries (Meredith et al., 2017).

Meteoric water shows seasonal ranges that typically span 2% – 5% (Figure 5). Values for F_{met} are typically higher than those for F_{sim} at any time during the sequence of measurements (Figure 5, second panel cf. first panel). This echoes results from a time series site further south along the WAP (in northern Marguerite Bay; Figure 1), and indicates the general dominance of meteoric water in setting the overall mean freshwater levels. The WAP-wide cruise data reflect this general meteoric water dominance also, though with some notable counter examples (Meredith et al., 2010, 2017).

As with sea ice melt, distinct interannual variability in meteoric water is present, with peak values varying from around 4% (2011/12; 2014/15) up to 5 or 6% (Figure 5). Superposed on this are many shallow extrema with high values of F_{met} ; these extend values up to 8% , and are exclusively from the surface water sampling

at Station B (Figure 5, lower panel). (Note that there are no surface F_{met} values at Station E that exceed 6%; however, the surface sampling at Station E is markedly less frequent than that at Station B).

Within the sampling conducted here, a recurring feature is the general increase in F_{met} during the first few months of each season (Figure 5). This is the converse of salinity (Figure 3), which has a tendency to decline over this period as freshwater is accumulated in the upper layers of the ocean. The F_{met} increase indicates that this freshening is normally dominated by meteoric water input (glacial melt, precipitation, runoff from melted snow), rather than sea ice melt. Melt of snow that accumulates on sea ice over winter could, in theory, contribute to the F_{met} increases over this period, but this would likely be paralleled by an increase in F_{sim} , which is mostly not a clear signal (Figure 5, upper panel). The extreme high values of F_{met} (>6%) are all in the later part of each sampling season (January to March; with none during October to December).

While the restriction of sampling to the summer window means that not all years have well-characterized peaks in F_{met} , when such peaks are present it is apparent that they have a tendency to occur 1–2 months after the peak in F_{sim} (Figure 5). This likely reflects the overall reservoir size for the freshwater components and the timing of their release into the water column, with sea ice having a tendency to be depleted first during the melt season while meteoric water input (in the form of glacial ice, snow, and precipitation) can persist longer.

4. Controls on Sea Ice Melt: Local- and Large-Scale Influences

As noted above, the mass balance shows that sea ice melt varies generally between around -2% and $+2\%$, suggesting that the region is in an approximate balance concerning sea ice formation and melt over the period 2012–2018. However, this does not inform on the spatial scales on which the processes affecting our derived F_{sim} are driven, or how these might change. To investigate this, we interpret the freshwater series presented above alongside the climatological and local meteorological data.

The strong peak in F_{sim} in 2013/14 was studied previously using the shelf-wide cruise data (Meredith et al., 2017) and attributed to northward wind anomalies that persisted during September and December 2013 in particular, resulting in a long ice season duration and a very late spring retreat of the ice edge (Figure 6). This tended to retain the sea ice in situ, allowing elevated levels of sea ice melt to become established as the melt period progressed. These findings were corroborated with time series data from adjacent to Rothera Research Station (Figure 1), emphasizing the large-scale relevance of the results. Significantly, Meredith et al. (2017) noted that the timing of the sea ice retreat (as opposed to the maximum winter sea ice extent preceding the melt period) was the key factor in controlling the elevation of F_{sim} .

This overall concept of the cause of high F_{sim} in 2013/14 is still consistent with the data from the more northward-located coastal sampling site used here, despite the broader WAP shelf region experiencing strong cyclonic winds in October, with southward winds causing an earlier ice edge retreat further offshore of this sampling site (Figure 6). However, the ice edge retreat at the WAP was thereafter slowed by more eastward to northward winds during November and particularly December. Thus, the concurrence of the high F_{sim} peak seen here with comparable anomalies seen in the shelf-wide cruise sampling and time series data at Rothera emphasizes that this high F_{sim} anomaly reflects a large- (WAP-wide) scale modulation of the sea ice field associated with anomalous northward wind forcing, particularly in the key month of December.

In our Palmer Station series, there is a second occurrence (2016/17) of values for F_{sim} that are as high as the peak values seen in 2013/14. This peak occurred earlier in the relevant season (December, as opposed to January; Figure 5), one consequence of which was that the shelf-wide cruise sampling that occurred in January 2017 did not capture it (not shown). Quasi-weekly time series data from Rothera Research Station (Figure 1) also do not show elevated F_{sim} in this season, indicating that the peak at Palmer Station is more localized than the 2013/14 peak (Meredith, 2019).

Our interpretation of the elevated F_{sim} in 2016/17 again relates to anomalous wind forcing, though of a profoundly different nature and scale. Figure 7 shows sea ice concentrations for the period September 2016 to February 2017, with wind anomaly vectors overlain. Of particular note are the strong south to south-eastward wind anomalies that persisted in September and October 2016; these anomalous winds pushed a rapid ice edge retreat and forced its location well south of its climatological mean position, where it

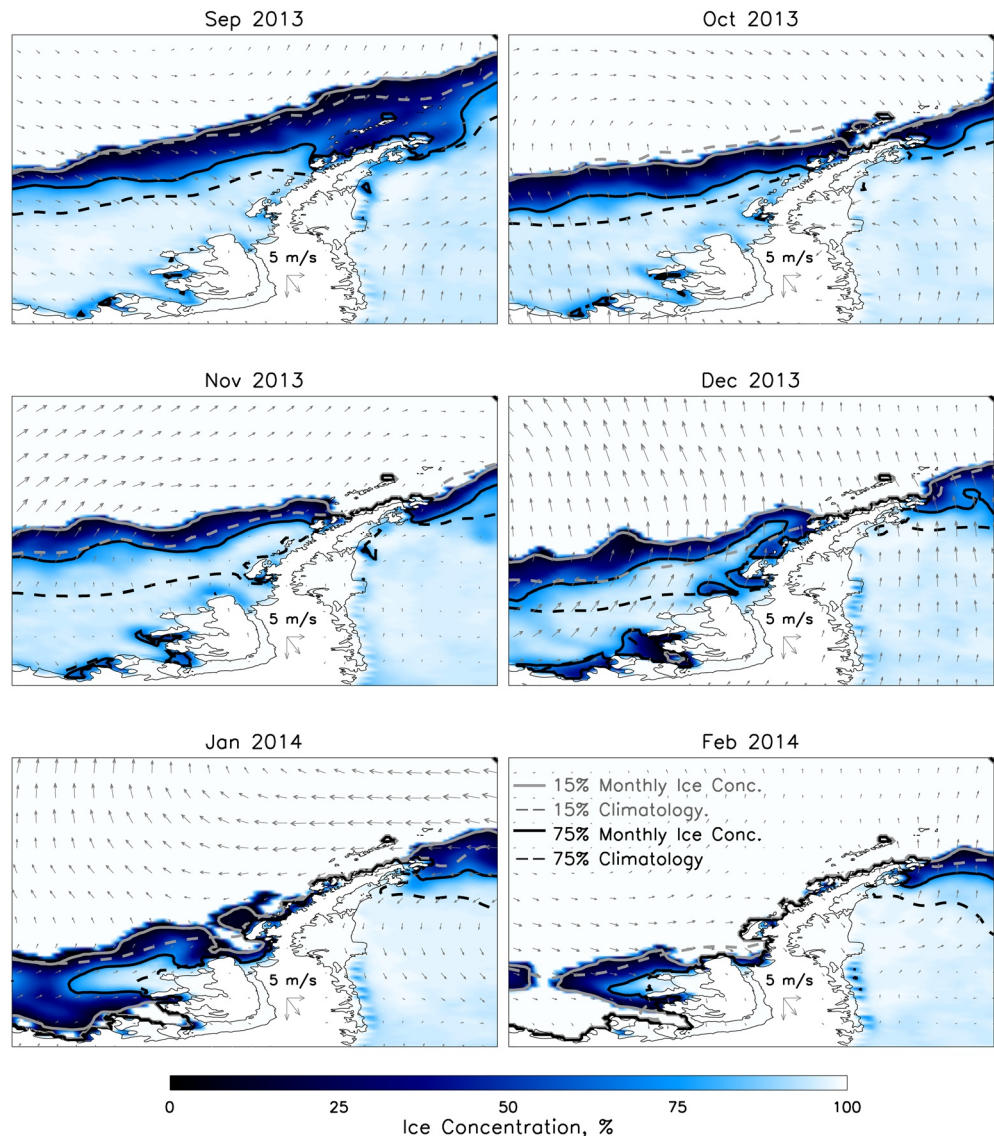


Figure 6. Monthly mean fields of sea ice concentration and wind speed anomaly for summer season 2013/14, from Scanning Multi-channel Microwave Radiometer-Special Sensor Microwave/Imager and ERA-Interim respectively (see Methods for details). Gray and black lines denote the ice edge defined by the 15% and 75% ice concentrations respectively, with the dashed line being the climatological mean for that month and the solid line being the observed ice edge. Note in particular the northward wind anomalies in September and December 2013, which held the sea ice edge north of its climatological mean as the melt season commenced and enabled stronger in situ melting to occur.

remained southward for the rest of the year, particularly in the southwest quadrant of the WAP. It may seem initially counterintuitive that these persistent southeastward winds, particularly in September, could create an anomaly in F_{sim} equivalent to that seen in 2013/14, especially when the winds were from an opposite direction. However, the critical factor in 2016/17 is the geographical fate of the wind-driven sea ice, which appears to have been compacted rapidly into the coastal WAP regions where it was mechanically thickened. This created a large volume of solid-phase sea ice available to be melted locally over time as the melt period commenced and progressed.

This interpretation is supported by high-resolution sea ice imagery (Figure 8), which shows a narrow sea ice field in late 2016 with a remarkably linear sea ice edge. This is consistent with rapid wind-driven compaction of the sea ice field, such as the one noted previously at the WAP (Massom et al., 2008). By contrast, late 2013 shows a much more uneven ice edge, consistent with persistent wind anomalies that led to divergence and

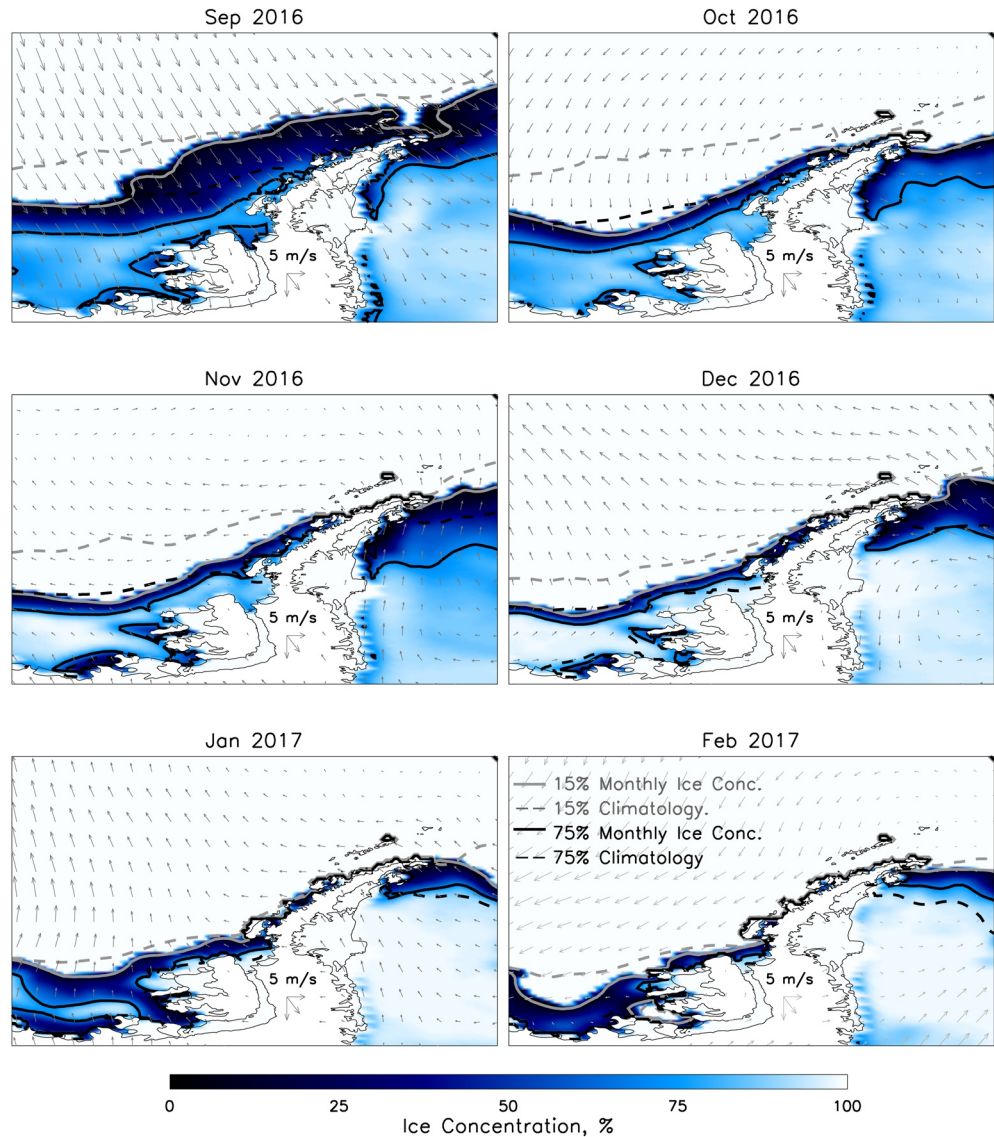


Figure 7. As for Figure 6 but for summer season 2016/17. Note in particular the southward/southeastward wind anomalies during September and October 2016, which compacted the sea ice into the coastal regions of the mid/northern west Antarctic Peninsula ahead of the melt season.

spreading of the sea ice field. While ice thickness measurements to corroborate the mechanical thickening in the coastal region are unavailable, further support from our interpretation derives from satellite-derived sea ice motion. This shows toward-land advection of ice throughout September 2016 (e.g., Figure 9), after which the band of ice becomes very narrow and almost motionless (not shown), that is, a thickened compacted ice cover becomes far less sensitive to wind-driven motion than an uncompacted thinner ice cover.

That the positive sea ice melt anomaly in 2016/17 is absent from the quasi-weekly time series data collected at Rothera (Figure 1; see also Meredith, 2019) may seem at odds with the linear ice edge extending across a large length of the WAP (Figure 8, lower panel) and wind-driven ice advection also spanning this scale (Figure 9, lower panel). However, the Rothera time series site is in northern Marguerite Bay and is shielded to the west by Adelaide Island. The high-resolution sea ice imagery (Figure 8) shows several patches of sea ice within Marguerite Bay at this time that had lower concentration than that of the general band of compacted sea ice along the WAP, likely partially a reflection of this more enclosed environment. The daily high-resolution sea ice images from November to January (not shown) also confirm that the more protected

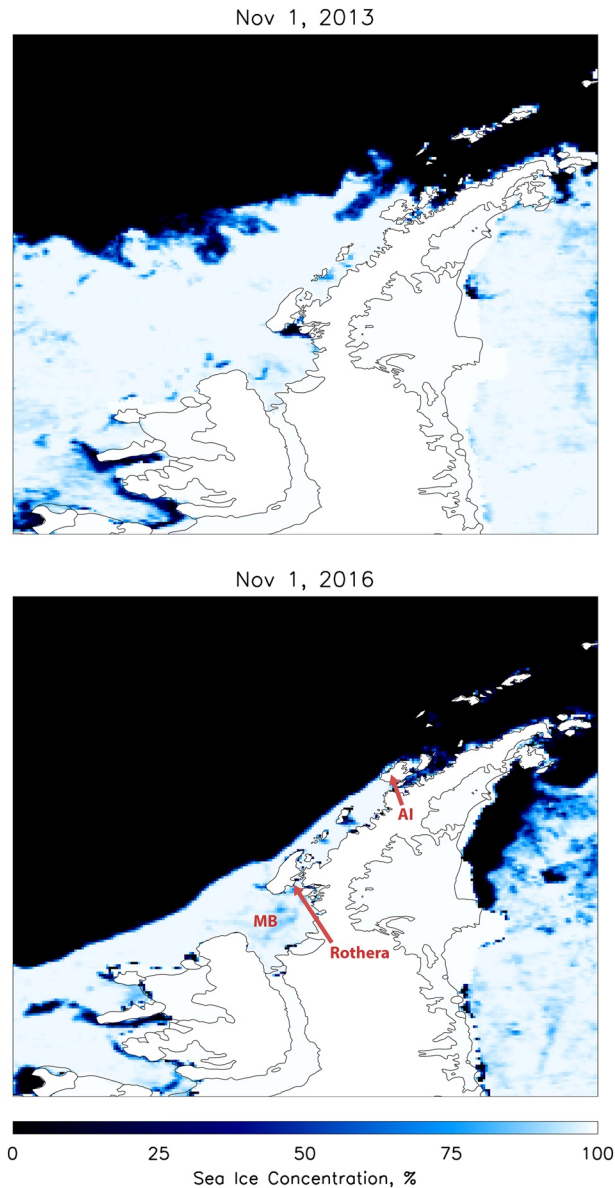


Figure 8. High-resolution sea ice concentration from Advanced Microwave Scanning Radiometer 2, for (top) November 1, 2013 and (bottom) November 1, 2016. Note in particular the very linear sea ice edge in November 2016, caused by wind-forced compaction of the sea ice to the coastal region of the West Antarctic Peninsula. By contrast, the sea ice edge in November 2013 was significantly less clearly delineated. Rothera, Marguerite Bay (MB), and Anvers Island (AI) are marked.

at Station B. This is the sampling site closest to land and the Marr Ice Piedmont (Figure 2), indicating that this is a very local-scale freshwater input. Candidate processes are the melt of snow that accumulates on land over winter, or surface/facial runoff from the glacier. Other possibilities are less compelling as explanations; for example, direct precipitation would be spread over a much broader area and thus feature at both sampling sites, as would melt of snow that had accumulated on top of sea ice. Further, while glacial melt from depth driven by intrusions of warm CDW can reach the surface in Antarctic coastal regions, in the form of upwelling buoyant plumes, this would be associated with pronounced mixing and would not be constrained to the very surface layer.

area adjacent to Rothera became ice-free much earlier than the southern portion of Marguerite Bay, the latter being more exposed to onshore winds, and thus more similar to the rest of the WAP coastal region which experienced anomalously late ice melt.

Overall, the difference in causality between the high F_{sim} events of 2013/14 and 2016/17 can be characterized as fundamentally a different phasing of the dynamic and thermodynamic sea ice responses to anomalous forcing. In 2013/14, the sea ice showed a marked dynamic response concurrent with a thermodynamic one, with the ice being retained largely in situ during the melt period. By contrast, in 2016/17 there was a strong dynamic response and subsequently a strong thermodynamic response, with marked ice advection ahead of its melting in the coastal regions. The location of our sampling station, adjacent to Anvers Island, appears to be sensitive to both of these phasings of the dynamic and thermodynamic sea ice response, that is, to both divergent (2013/14) and convergent (2016/17) wind forcing. (Note that we do not have the surface ocean velocity information from which the role of the ocean in influencing the sea ice response can be assessed; nonetheless, the consistency between the wind fields, ice motion, and ice melt indicates that this latter influence acted in tandem with the atmospheric forcing or had little effect on the overall net response).

Previously, periods of anomalous winds at the WAP and the changes in freshwater composition that they induce have been related to coupled modes of climate variability including the Southern Annular Mode (SAM) and the El Niño/Southern Oscillation (ENSO) phenomenon (Marshall, 2003; Meredith et al., 2013, 2017; Stammerjohn et al., 2008; Thompson & Wallace, 2000; van Wessem et al., 2017). We note that the rapid retreat of sea ice in late 2016 coincided with a very strong negative SAM, which was at its lowest in November since 1968 (Turner et al., 2017). It also coincided with a deepening of the Amundsen Sea Low, a large-scale atmospheric pattern that spans this part of Antarctica, and which modulates meridional winds west of the Antarctic Peninsula. This reinforces the concept that large-scale modes of climate variability exert pronounced influence on the distributions of freshwater at the WAP; our results here have demonstrated significant new complexity in the spatial scales of the response of sea ice melt.

5. Controls on Meteoric Water: Local- and Large-Scale Influences

5.1. Extreme Peaks in Surface Meteoric Water

The extrema in meteoric water (black dots in Figure 5) elevate the seasonal peaks of F_{met} by up to an additional 2%. Notably, they occur almost exclusively in the surface sampling (not at 10 m or the SWI at 5.8 m) and

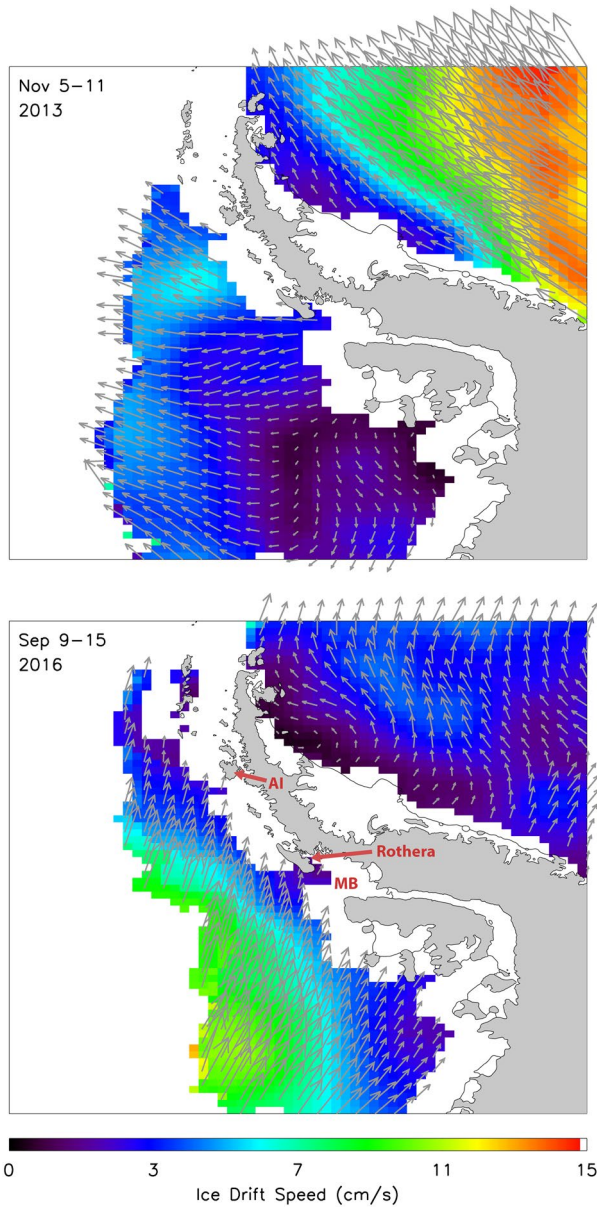


Figure 9. Vectors of weekly sea ice motion from the Polar Pathfinder 25 km EASE-Grid data, for (top) November 5–11, 2013 and (bottom) September 9–15, 2016. The speeds of sea ice motion are colored as background. Rothera, Marguerite Bay (MB), and Anvers Island (AI) are marked.

Of the cluster of samples with $\delta^{18}\text{O}$ less than -0.75‰ (Figure 3; third panel), all but one coincided with a mixed layer shallower than 10 m depth. This is unsurprising, since freshwater is the controlling term in the equation of state at low temperature, and hence fresh layers add greatly to stratification and upper-ocean stability. That these extrema are only ever seen in meteoric water (not sea ice melt; Figure 5) indicates that the freshwater injection in this form actively creates these layers, and the observations are not reflecting simple freshwater accumulation in an already-established stable stratification.

Also of relevance in the MLD data is that, while the general mixed layers are shallower than 50 m, there are occasional deep spikes that lower the mixed layer to 90 m or more (Figure 3). These occur predominantly at Station B, again closest to land and the proximate glacier. There are several processes that could cause these deepening events, including wind-induced coastal upwelling and the influence of internal tides, such as have been investigated in detail at Rothera (Wallace et al., 2008). It is not our intention to explore these in detail here, but we note that such occurrences would disrupt the shallow surface layers when present.

Overall, we derive a picture of irregular pulses of meteoric water building stratified layers which can be disrupted periodically by mixing events. This has biogeochemical and ecological significance: for example, if the freshwater layers contain micronutrients, it is beneficial to their fertilization of the local phytoplankton blooms that this water is injected into the euphotic zone. Conversely, mixing events would distribute surface-injected freshwater over a greater vertical range and affect the fate of any geochemical substances associated with it. Upper water column stability is critical in initiating phytoplankton blooms in this region (Carvalho et al., 2016; Schofield et al., 2017)

Against this background, it is worth noting that mixed layer deepening does not appear to be the same pronounced control on interannual variability in upper-ocean freshwater that is observed at the Rothera time series (Meredith et al., 2010, 2017). Close to Rothera, interannual changes in the seasonal upward entrainment of CDW is a dominant factor in controlling the upper-layer freshwater content. The deep mixed layers that can be observed at Rothera (down to 150 m in some winters) are a combination of buoyancy forcing in winter, especially related to sea ice processes, and wind-driven mixing. The latter process becomes markedly more effective in the absence of persistent fast ice during winter (Venables & Meredith, 2014). It is clear that the environs of Palmer Station are not exposed to the same level of extreme forcing by these processes as is Rothera.

5.2. Seasonal and Interannual Changes in Meteoric Water

Concurrent with the local-scale, intermittent injections of freshwater noted above are distinct seasonal and interannual changes in meteoric water content that occur at each of the Palmer Station sites and each of the depth levels sampled (Figure 5). The seasonality of F_{met} is such that it typically peaks in the January–March window, while the peak precipitation period at the WAP is typically during winter. This phase difference potentially reflects a combination of processes, including large-scale melt of accumulated snow from land along the length of the WAP, seasonality in glacial discharge, and the melt of snow on sea ice. We examine

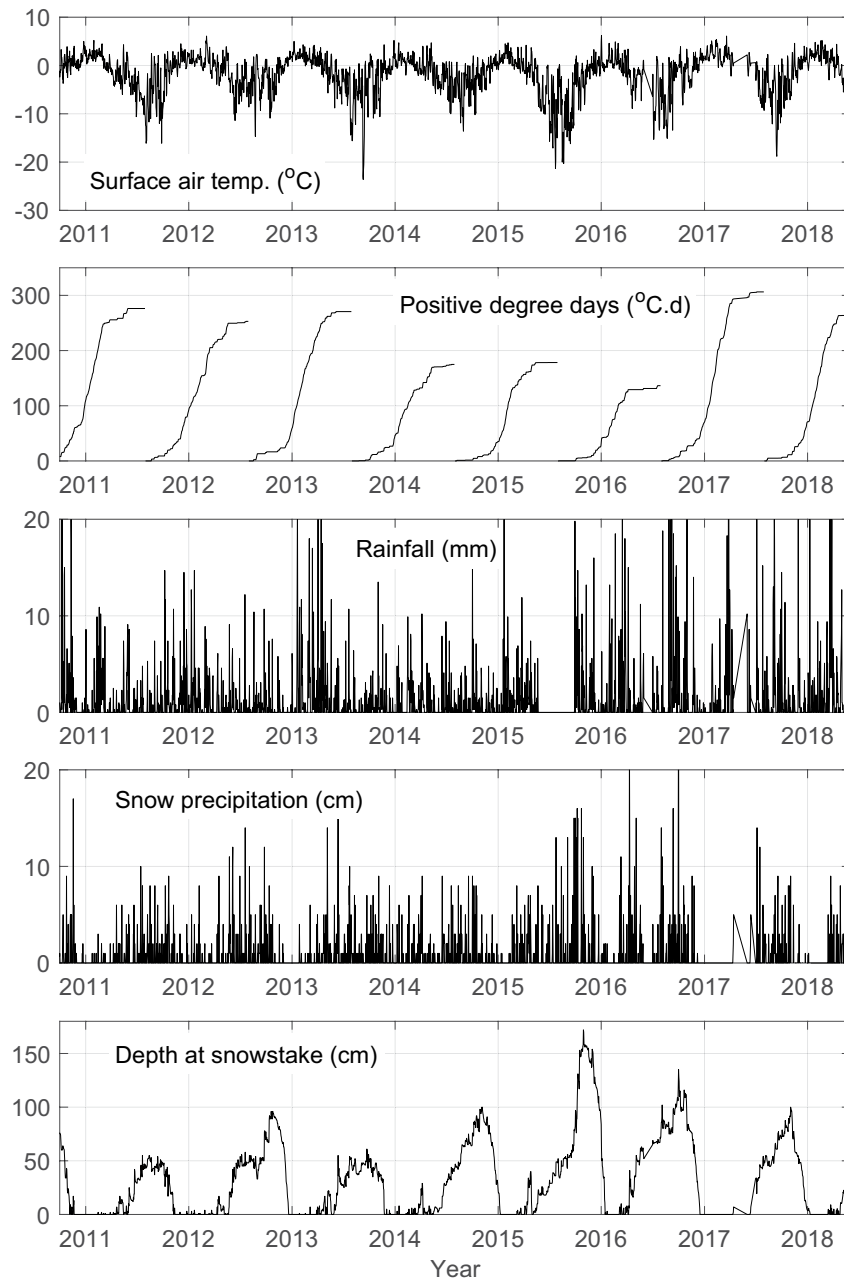


Figure 10. Series of meteorological data from Palmer Station, Anvers Island, relevant to the freshwater balance.

these possibilities here to gain insight into which is the most important in determining the seasonal and interannual variability of our meteoric water series.

With regard to the accumulation and melt of snow on land, snowstake measurements at Palmer Station show clearly the seasonal cycle in this, with pronounced accumulation occurring from around April/May and melt occurring typically during October to December (Figure 10). This reflects well the timing of the seasonal increase in F_{met} (Figure 5).

On interannual timescales, distinct changes in meteoric water concentration close to Palmer Station are present in our series (Figure 5, third panel), with 2011/12 showing the lowest seasonal peak (around 4%) and 2016/17 the highest (around 6%). Previously, we explained interannual variability in meteoric water concentrations across the WAP shelf as seen in January cruise data by relating the changes seen in precipitation

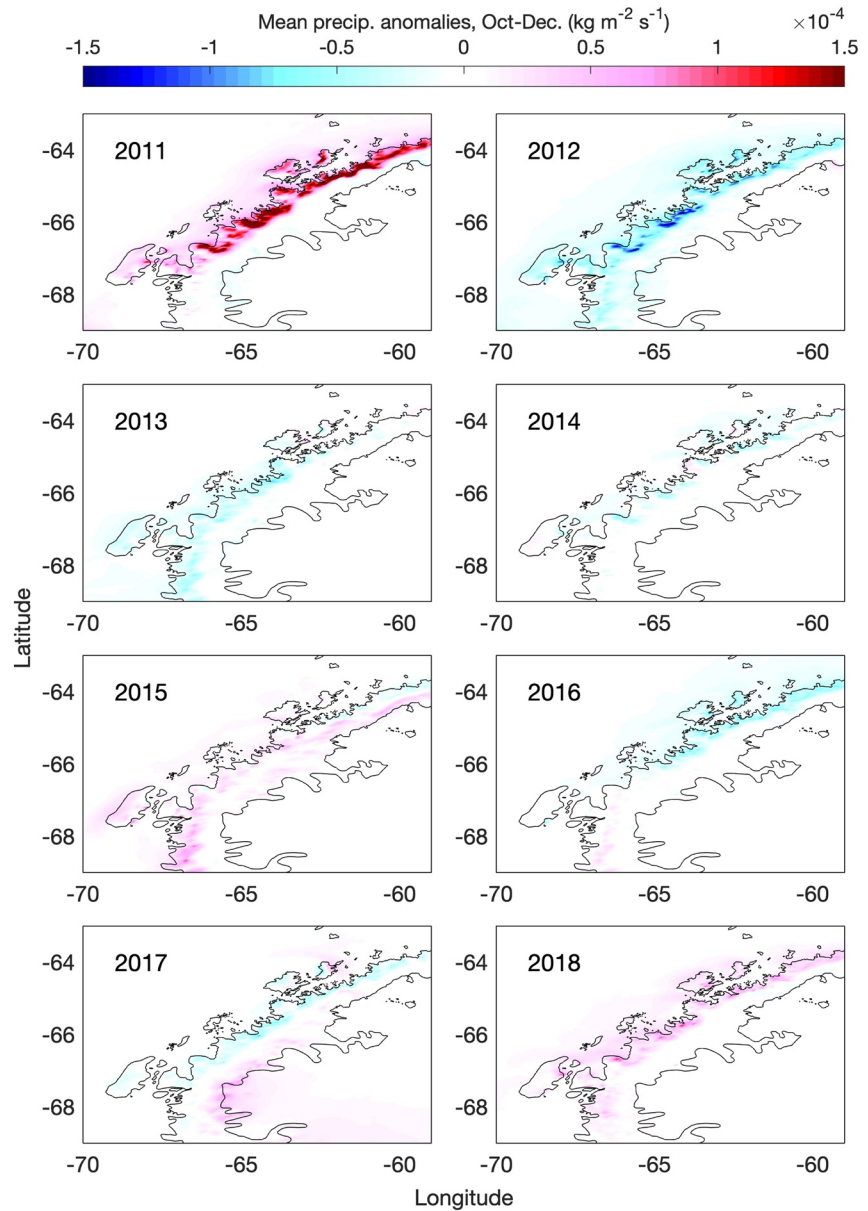


Figure 11. Anomalies in precipitation at the Antarctic Peninsula in Regional Atmospheric Climate Model 2 ($\text{kg m}^{-2} \text{s}^{-1}$), covering the period 2011 to 2018. Months October to December are used here, being the period used previously in explaining the shelf-wide meteoric water anomalies observed in January cruise data (Meredith et al., 2017).

anomalies taken over the last 3 months of the preceding year (Meredith et al., 2017). Such anomalies, derived from RACMO2, are shown here in Figure 11, and it is clear that the relationship previously established breaks down for the Palmer Station series, with the highest rates of precipitation occurring in late 2011, and comparatively low rates in 2016.

Instead, we demonstrate here that a better relationship is obtained by considering precipitation over the winter period (April to October) that precedes the seasonal peak in F_{met} at Palmer Station (Figure 12). The choice of this window is based on the snowstake measurements at Palmer Station, which inform on the period during which snow accumulates on land and subsequently melts (Figure 10). When precipitation anomalies are averaged over this seasonal window (Figure 12), it is clear that 2011 featured moderately strong negative anomalies at Palmer Station, while 2016 showed distinct positive anomalies: these coincide

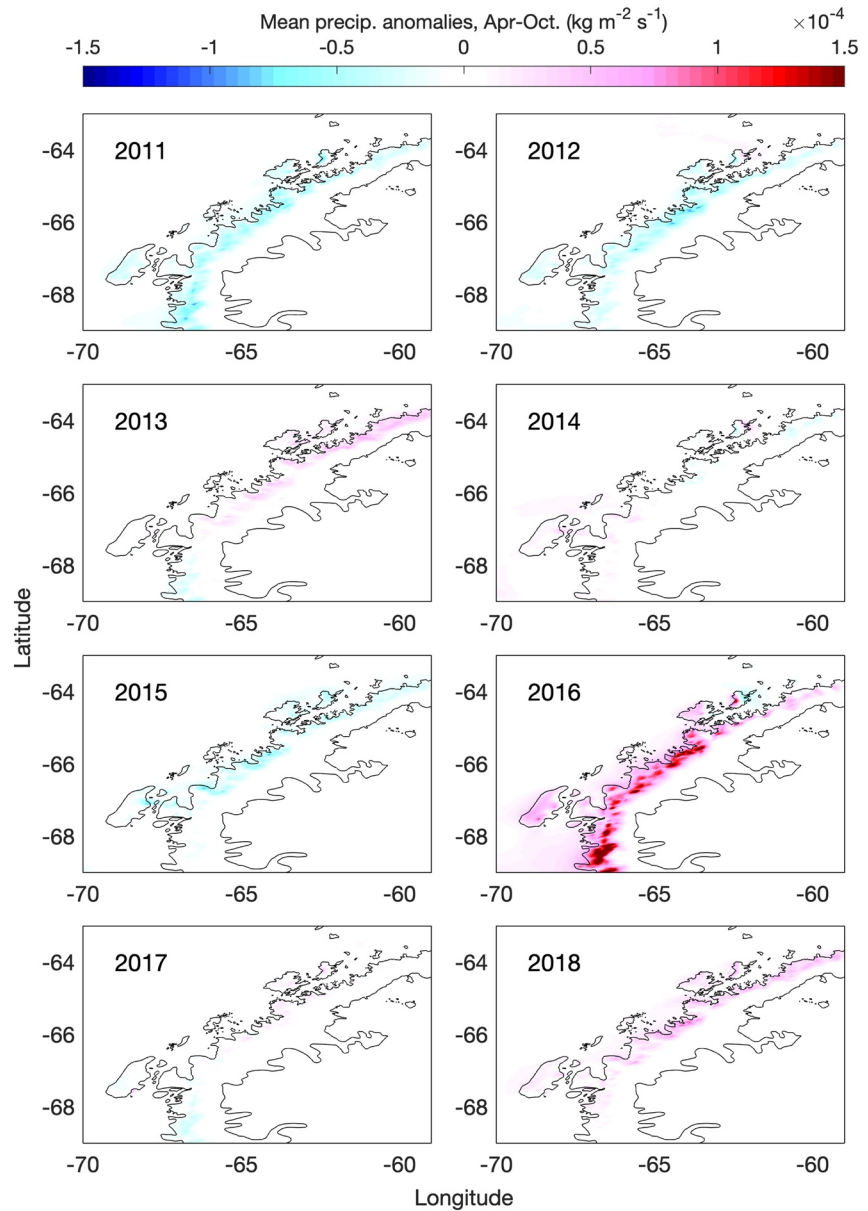


Figure 12. Anomalies in precipitation at the Antarctic Peninsula in Regional Atmospheric Climate Model 2 ($\text{kg m}^{-2} \text{s}^{-1}$), covering the period 2011 to 2018. Months April to October are used here, being the general period over which precipitation tends to accumulate on land/sea ice during winter ahead of the spring melt season (see Figure 10).

well with the interannual changes in meteoric water. Other years lie intermediate between these extremes, though with complexity due to combined processes; for example, 2012 showed anomalously low precipitation in RACMO2 (Figure 12) which resulted in generally low F_{met} at Palmer Station in 2012/13 (Figure 5, third panel) that was elevated at the very end of the sampling season by a burst of direct precipitation (Figure 10).

Overall, while correlations are not possible due to the small number of years of data, a greatly improved relationship is seen, indicating that changes in the winter accumulation of precipitation is generally a more important control on the peak level of F_{met} seen at Palmer Station the following summer than is direct precipitation in spring. The precipitation anomalies are coherent in a band along much of the WAP coast (Figure 12), suggesting that while local accumulation is a key factor, this process likely occurs similarly over larger scales and will influence freshwater concentrations coherently along much of the coastal ocean.

General southward transport in the WAP coastal circulation will aggregate the inputs and transport them poleward (Moffat et al., 2008), thus integrating the local signals over much larger scales.

We thus find that a key factor influencing interannual changes in F_{met} at Palmer Station site is that different amounts of accumulated snow build up over winter and are available to melt during spring and summer, thus injecting comparatively large amounts of meteoric water into the coastal ocean over relatively short periods. In addition, advection of water that has been similarly influenced from along the WAP coast will be an important factor, and while Anvers Island is typically thought to be close to the head of the southward-flowing Antarctic Peninsula Coastal Current (Moffat et al., 2008), the injection and integration of this freshwater will be an important influence on its transport and properties.

While the relationship between precipitation and F_{met} succeeds in explaining some of the most pronounced anomalies in the series, it is inevitably not perfect. Some of this is due to the fact that accumulated precipitation represents the potential for seasonal meteoric water input to the ocean, but the actual input depends also on the evolution of local melt conditions at the sites of input. Local meteorological data recorded at Palmer Station give some insight into this. The snowstake measurements (accumulated snow; Figure 12) show strong interannual variations, including comparatively low accumulation in winter 2011, which preceded the lowest seasonal F_{met} peak in the ocean time series, and much higher levels during the winter of 2016 prior to comparatively higher seasonal peak in F_{met} in 2016/17. However, the highest accumulated snow occurred in 2015, and while F_{met} in 2015/16 was higher than in 2011/12, it was not as high as in 2016/17. The potential for melt, as expressed by PDD, goes some way to explaining this difference: PDD was actually the lowest within our series in 2015/16, and the highest in 2016/17 (Figure 10). Thus we observe that the accumulation and seasonal discharge of snow at the coastal WAP, with the latter modulated by interannual changes in melt potential, are key processes that determine interannual changes in meteoric water concentrations at Palmer Station.

We find that other processes considered are less influential in determining the seasonal and interannual changes in our meteoric water time series. Concerning glacial melt, and specifically that driven by atmospheric or surface ocean heat (Figure 3, upper panel; Figure 10), we note that the series of surface temperature or PDD by themselves do not adequately explain variations in F_{met} (Figure 5 cf. Figure 12). Further, glacial melt at depth driven by warm CDW is unlikely in the vicinity of our sampling site, since the local ice masses are notably shallow- or land-terminating, with maximum grounding depths of just a few tens of meters (Figure 2). This does not negate the quantitative importance of glacial discharge in the temporal-mean freshwater balance of our study area, or the WAP more generally, but it does argue against it being the dominant process in controlling the variability in meteoric water as measured.

A different process that could potentially contribute to the changes in meteoric water is the seasonal accumulation and melt of snow on sea ice, and interannual changes therein. This is multi-faceted process that is not well constrained by data, however if it were to dominate we would expect a significant relationship to exist between the meteoric water and the sea ice melt as quantified in our series. Such a relationship is absent, with the seasonal phase of these series and their interannual changes not coinciding (Figure 5). Significant work would be required to investigate this further; on the basis of existing information, however, this does not appear to be a leading-order process that determines our meteoric water series.

6. Summary and Conclusions

We have observed marked variability in the freshwater balance of the coastal WAP adjacent to Anvers Island. Interannual variability is driven by both sea ice and meteoric freshwater sources, and in both cases a range of spatial scales are inferred to be important in driving the variability. It is important to deconvolve this complexity, in order to better understand the totality of the causal factors and hence move toward better predictive skill.

In relation to sea ice melt, the results confirm the large-scale impact of anomalous northward winds in late 2013, which resulted in a late sea ice retreat and anomalously high sea ice melt concentrations across the WAP shelf in early 2014. Intriguingly, a similarly high level of sea ice melt is observed in late 2016, despite wind anomalies of a very different direction. We have shown that this second instance was caused by sea

ice being compacted and mechanically thickened in the coastal regions of the WAP, and thus constituting a large reservoir of freshwater that was released locally when the melt season began. In essence, there is a complex balance and interplay between the dynamic and thermodynamic influences on the derived sea ice melt concentrations, each of which maps onto different spatial scales. This adds complexity and challenges the development of simple predictive relationships.

We infer that, despite having similar magnitudes of sea ice melt at Anvers Island in these two seasons, the spatial scale of anomalies of these events across the WAP will be markedly different. While this cannot be assessed using the data from the January cruises at the WAP (since the 2016 anomaly had passed by early 2017), this is consistent with the causal mechanisms deduced above and is lent support by the absence of the 2016 signal in the time series at Rothera (northern Marguerite Bay). We have shown that the $\delta^{18}\text{O}$ sampling at Palmer Station is sensitive to both these scales, and correct determination of the sea ice melt changes is required in order to reliably attribute their local biogeochemical and ecological consequences.

The coastal meteoric water budget is seen to possess even more complexity across a range of spatial scales. Very locally, shallow layers of elevated meteoric water are seen close to the Marr Ice Piedmont adjacent to Palmer Station, which we deduce are caused by glacial runoff and/or snow melt in thin surface layers. These freshwater pulses cause intermittent enhancement in stable upper-ocean stratification, which is destroyed periodically, most likely by mixing events close to the coastal boundary.

We have observed that seasonal peaks in meteoric water have a tendency to occur 1–2 months after the peaks in sea ice melt. This is likely a consequence of differences in the overall reservoir size for these freshwater components, with sea ice having a tendency to be depleted first during the melt season while meteoric water input (in the form of glacial ice and snow, augmented with any direct precipitation) can persist longer. This has consequences for the physical and biogeochemical functioning of the coastal ocean; while the physical effects (e.g., stabilization of the upper ocean) may appear similar, the geochemical composition of these freshwater sources differs greatly.

Further, we have observed distinct interannual changes to the seasonal peaks of meteoric water concentration, and attributed them to changes in the amount of accumulated snow the preceding winter, combined with local melt potential from seasonal atmospheric warming. These mechanisms are dependent on the immediate proximity of a coastal boundary that can store freshwater for seasonal release during the melt season, and differ from the large-scale, WAP-wide mechanisms described previously. Input of freshwater to the coastal ocean at the WAP is important in driving a southward-flowing coastal current; this will integrate inputs along the length of its flow, and generate cross-shelf gradients in properties.

It has been noted previously that precipitation at the WAP is sensitive to large-scale modes of climate variability, including ENSO and SAM (van Wessem et al., 2017), and that this has the potential to build predictive skill if the future trajectories of these modes can be projected with some level of confidence. With our comparatively short time series, we cannot address directly the influence of such climate modes as forcing factors on our ocean meteoric water concentrations. However, to the extent that the precipitation anomalies observed here are known to be dependent on such coupled modes and have been shown to be causal in explaining our interannual changes in meteoric water, this connects our local-scale observations of change to very large scale (circumpolar and hemispheric) forcing. Further, SAM is known to be sensitive to anthropogenic influences, via greenhouse gas emissions and ozone depletion (Marshall, 2003; Thompson et al., 2000), creating a possible link whereby human-induced changes could influence the meteoric water component of the WAP coastal freshwater budget. However, our new results demonstrate notable complexity in the freshwater responses across a range of scales, and emphasize the need to carefully understand such responses if attribution is to be reliable and such predictive skill is to be enhanced.

Data Availability Statement

Data used here are publicly available. The Palmer LTER ocean data used here are available via the Environmental Data Initiative (EDI) data portal at <https://portal.edirepository.org/nis/mapbrowse?packageid=knb-lter-pal.309.1> (10.6073/pasta/251000bc5fdcc5f11ad975295dd38774). The Palmer Station meteorological data are available via the EDI data portal at <https://portal.edirepository.org/nis/meta->

[dataviewer?packageid=knb-lter-pal.214.3](#). The RACMO2 output used here is available via van Wessem et al. (2018) and at https://www.projects.science.uu.nl/iceclimate/publications/data_2021.php. The SMMR/SSMI sea ice data are available via the EOS Distributed Active Archive Center (DAAC) at the National Snow and Ice Data Center, University of Colorado at Boulder: <https://nsidc.org/data/NSIDC-0051/versions/1>. AMSR2 sea ice data are available from the Universität Bremen (<https://www.seaice.uni-bremen.de>). ECMWF ERA-Interim reanalysis data are available through Dee et al. (2011) and at <https://www.ecmwf.int/en/forecasts/datasets/reanalysis-datasets/era-interim>.

Acknowledgments

The authors thank the anonymous reviewers for constructive comments that helped improve this manuscript. John Kerfoot and Carleen Tijm Reijmer are sincerely thanked for data archiving. Meredith, Brearley, Barham, Venables, Leng, and Arrowsmith received support from the NERC-funded ORCHESTRA program; Meredith, Brearley, Barham, and Venables received support from the NERC National Capability-Single Centre scheme. This project also received funding from the EU's Horizon 2020 research and innovation program under the grant agreement No. 821001. Laura Gerrish is thanked for cartographic input. Isotope sampling was supported by the US NSF Office of Polar Program grants OPP-08-23101 and PLR-14-0435 (Palmer LTER); the authors thank all who contributed to the sample collection, including the Antarctic Research Consortium for logistics, boating and laboratory support. Palmer LTER also supported the participation of Stammerjohn, Ducklow, Schofield, and Waite in this research. Naomi Manahan and Rich Iannuzzi (LDEO) are thanked for coordinating sampling and logistics, and for data processing.

References

Annett, A. L., Fitzsimmons, J. N., Séguret, M. J. M., Lagerström, M., Meredith, M. P., Schofield, O., & Sherrell, R. M. (2017). Controls on dissolved and particulate iron distributions in surface waters of the Western Antarctic Peninsula shelf. *Marine Chemistry*, *196*, 81–97. <https://doi.org/10.1016/j.marchem.2017.06.004>

Banwell, A. F., Datta, R. T., Dell, R. L., Moussavi, M., Brucker, L., Picard, G., et al. (2020). 32-year record-high surface melt in 2019/2020 on north George VI Ice Shelf, Antarctic Peninsula. <https://doi.org/10.5194/tc-2020-309>

Barrand, N. E., Vaughan, D. G., Steiner, N., Tedesco, M., Kuipers Munneke, P., van den Broeke, M. R., & Hosking, J. S. (2013). Trends in Antarctic Peninsula surface melting conditions from observations and regional climate modeling. *Journal of Geophysical Research: Earth Surface*, *118*, 315–330. <https://doi.org/10.1029/2012JF002559>

Boyd, P. W., & Ellwood, M. J. (2010). The biogeochemical cycle of iron in the ocean. *Nature Geoscience*, *3*, 675–682. <https://doi.org/10.1038/ngeo964>

Bracegirdle, T. J. (2013). Climatology and recent increase of westerly winds over the Amundsen Sea derived from six reanalyses. *International Journal of Climatology*, *33*, 843–851. <https://doi.org/10.1002/joc.3473>

Cape, M. R., Vernet, M., Pettit, E. C., Wellner, J., Truffer, M., Akie, G., et al. (2019). Circumpolar Deep Water impacts glacial meltwater export and coastal biogeochemical cycling along the West Antarctic Peninsula. *Frontiers in Marine Science*, *6*, 144. <https://doi.org/10.3389/fmars.2019.00144>

Carvalho, F., Kohut, J., Oliver, M. J., & Schofield, O. (2017). Defining the ecologically relevant mixed-layer depth for Antarctica's coastal seas. *Geophysical Research Letters*, *44*(44), 338–345. <https://doi.org/10.1002/2016GL071205>

Carvalho, F., Kohut, J., Oliver, M. J., Sherrell, R. M., & Schofield, O. (2016). Mixing and phytoplankton dynamics in a submarine canyon in the West Antarctic Peninsula. *Journal of Geophysical Research: Oceans*, *121*(7), 5069–5083. <https://doi.org/10.1002/2016JC011650>

Comiso, J. C. (2000). Bootstrap sea ice concentrations from Nimbus-7 SMMR and DMSP SSM/I-SSMIS, Version 2. Boulder, CO: NASA National Snow and Ice Data Center Distributed Active Archive Center.

Comiso, J. C., & Nishio, F. (2008). Trends in the sea ice cover using enhanced and compatible AMSR-E, SSM/I, and SMMR data. *Journal of Geophysical Research*, *113*, C02S07. <https://doi.org/10.1029/2007JC004325>

Cook, A. J., Fox, A. J., Vaughan, D. G., & Ferrigno, J. G. (2005). Retreating glacier fronts on the Antarctic Peninsula over the past half-century. *Science*, *308*(5721), 541–544. <https://doi.org/10.1126/science.1104235>

Cook, A. J., Holland, P. R., Meredith, M. P., Murray, T., Luckman, A., & Vaughan, D. G. (2016). Ocean forcing of glacier retreat in the western Antarctic Peninsula. *Science*, *353*(6296), 283–286. <https://doi.org/10.1126/science.aae0017>

Corbett, D. R., Crenshaw, J., Null, K., Peterson, R. N., Peterson, L. E., & Lyons, W. B. (2017). Nearshore mixing and nutrient delivery along the western Antarctic Peninsula. *Antarctic Science*, *29*(5), 397–409. <https://doi.org/10.1017/S095410201700013X>

Dee, D. P., Uppala, S. M., Simmons, A. J., Berrisford, P., Poli, P., Kobayashi, S., et al. (2011). The ERA-Interim reanalysis: Configuration and performance of the data assimilation system. *Quarterly Journal of the Royal Meteorological Society*, *137*, 553–597. <https://doi.org/10.1002/qj.828>

Dierssen, H. M., Smith, R. C., & Vernet, M. (2002). Glacial meltwater dynamics in coastal waters west of the Antarctic Peninsula. *Proceedings of the National Academy of Sciences of the United States of America*, *99*(4), 1790–1795. <https://doi.org/10.1073/pnas.032206999>

Duprat, L. P. A. M., Bigg, G. R., & Wilton, D. J. (2016). Enhanced Southern Ocean marine productivity due to fertilization by giant icebergs. *Nature Geoscience*, *9*(3), 219–221. <https://doi.org/10.1038/ngeo2633>

Harangozo, S. A. (2006). Atmospheric circulation impacts on winter maximum sea ice extent in the west Antarctic Peninsula region (1979–2001). *Geophysical Research Letters*, *33*(L02502). <https://doi.org/10.1029/2005GL024978>

Hawkings, J. R., Wadhwa, J. L., Tranter, M., Raiswell, R., Benning, L. G., Statham, P. J., et al. (2014). Ice sheets as a significant source of highly reactive nanoparticulate iron to the oceans. *Nature Communications*, *5*(3929). <https://doi.org/10.1038/ncomms4929>

Henley, S. F., Schofield, O. M., Hendry, K. R., Schloss, I. R., Steinberg, D. K., Moffat, C., et al. (2019). Variability and change in the west Antarctic Peninsula marine system: Research priorities and opportunities. *Progress in Oceanography*, *173*, 208–237. <https://doi.org/10.1016/j.pocean.2019.03.003>

King, J. C. (1994). Recent climate variability in the vicinity of the Antarctic Peninsula. *International Journal of Climatology*, *14*, 357–369. <https://doi.org/10.1002/joc.3370140402>

Kirchgäßner, A. (2011). An analysis of precipitation data from the Antarctic base Faraday/Vernadsky. *International Journal of Climatology*, *31*, 404–414. <https://doi.org/10.1002/joc.2083>

Li, X., Holland, D. M., Gerber, E. P., & Yoo, C. (2014). Impacts of the north and tropical Atlantic Ocean on the Antarctic Peninsula and sea ice. *Nature*, *505*, 538–542. <https://doi.org/10.1038/nature12945>

Marshall, G. J. (2003). Trends in the southern annular mode from observations and reanalyses. *Journal of Climate*, *16*, 4134–4143. [https://doi.org/10.1175/1520-0442\(2003\)016<4134:titsam>2.0.co;2](https://doi.org/10.1175/1520-0442(2003)016<4134:titsam>2.0.co;2)

Martinson, D. G., & McKee, D. C. (2012). Transport of warm Upper Circumpolar Deep Water onto the western Antarctic Peninsula continental shelf. *Ocean Science*, *8*(4), 433–442. <https://doi.org/10.5194/os-8-433-2012>

Massom, R. A., Stammerjohn, S. E., Lefebvre, W., Harangozo, S. A., Adams, N., Scambos, T. A., et al. (2008). West Antarctic Peninsula sea ice in 2005: Extreme ice compaction and ice edge retreat due to strong anomaly with respect to climate. *Journal of Geophysical Research*, *113*(C2), C02S20. <https://doi.org/10.1029/2007JC004239>

Meredith, M. P. (2019). The global importance of the Southern Ocean and the key role of its freshwater cycle. *Ocean Challenge*, *23*(2), 27–32.

- Meredith, M. P., Brandon, M. A., Wallace, M. I., Clarke, A., Leng, M. J., Renfrew, I. A., et al. (2008). Variability in the freshwater balance of northern Marguerite Bay, Antarctic Peninsula: Results from $\delta^{18}O$. *Deep-Sea Research Part II: Topical Studies in Oceanography*, 55, 309–322. <https://doi.org/10.1016/j.dsr2.2007.11.005>
- Meredith, M. P., Falk, U., Bers, A. V., Mackensen, A., Schloss, I. R., Ruiz Barlett, E., et al. (2018). Anatomy of a glacial meltwater discharge event in an Antarctic cove. *Philosophical Transactions of the Royal Society A*, 376(2122), 20170163. <https://doi.org/10.1098/rsta.2017.0163>
- Meredith, M. P., & King, J. C. (2005). Rapid climate change in the ocean west of the Antarctic Peninsula during the second half of the 20th century. *Geophysical Research Letters*, 32, L19604. <https://doi.org/10.1029/2005GL024042>
- Meredith, M. P., Sommerkorn, M., Cassotta, S., Derksen, C., Ekaykin, A., Hollowed, A., et al. (2019). Polar regions. In H.-O. Portner, D. C. Roberts, V. Masson-Delmotte, P. Zhai, M. Tignor, E. Poloczanska, et al. (Eds.), *IPCC special report on the ocean and cryosphere in a changing climate* (pp. 203–320).
- Meredith, M. P., Stammerjohn, S. E., Venables, H. J., Ducklow, H. W., Martinson, D. G., Iannuzzi, R. A., et al. (2017). Changing distributions of sea ice melt and meteoric water west of the Antarctic Peninsula. *Deep-Sea Research Part II: Topical Studies in Oceanography*, 139, 40–57. <https://doi.org/10.1016/j.dsr2.2016.04.019>
- Meredith, M. P., Venables, H. J., Clarke, A., Ducklow, H. W., Erickson, M., Leng, M. J., et al. (2013). The freshwater system west of the Antarctic Peninsula: Spatial and temporal changes. *Journal of Climate*, 26, 1669–1684. <https://doi.org/10.1175/JCLI-D-12-00246.1>
- Meredith, M. P., Wallace, M. I., Stammerjohn, S. E., Renfrew, I. A., Clarke, A., Venables, H. J., et al. (2010). Changes in the freshwater composition of the upper ocean west of the Antarctic Peninsula during the first decade of the 21st century. *Progress in Oceanography*, 87, 127–143. <https://doi.org/10.1016/j.poccean.2010.09.019>
- Mitchell, B. G., & Holm-Hansen, O. (1991). Observations of modeling of the Antarctic phytoplankton crop in relation to mixing depth. *Deep-Sea Research Part A. Oceanographic Research Papers*, 38, 981–1007. [https://doi.org/10.1016/0198-0149\(91\)90093-u](https://doi.org/10.1016/0198-0149(91)90093-u)
- Moffat, C., Beardsley, R. C., Owens, B., & van Lipzig, N. (2008). A first description of the Antarctic Peninsula Coastal Current. *Deep-Sea Research Part II: Topical Studies in Oceanography*, 55(3–4), 277–293. <https://doi.org/10.1016/j.dsr2.2007.10.003>
- Moline, M. A., Claustre, H., Frazer, T. K., Schofield, O., & Vernet, M. (2004). Alteration of the food web along the Antarctic Peninsula in response to a regional warming trend. *Global Change Biology*, 10(12), 1973–1980. <https://doi.org/10.1111/j.1365-2486.2004.00825.x>
- Montes-Hugo, M., Doney, S. C., Ducklow, H. W., Fraser, W., Martinson, D., Stammerjohn, S. E., & Schofield, O. (2009). Recent changes in phytoplankton communities associated with rapid regional climate change along the western Antarctic Peninsula. *Science*, 323(5920), 1470–1473. <https://doi.org/10.1126/science.1164533>
- Östlund, H. G., & Hut, G. (1984). Arctic Ocean water mass balance from isotope data. *Journal of Geophysical Research*, 89, 6373–6381. <https://doi.org/10.1029/jc089ic04p06373>
- Parkinson, C. L. (2019). A 40-y record reveals gradual Antarctic sea ice increases followed by decreases at rates far exceeding the rates seen in the Arctic. *Proceedings of the National Academy of Sciences of the United States of America*, 116(29), 14414–14423. <https://doi.org/10.1073/pnas.1906556116>
- Pritchard, H. D., & Vaughan, D. G. (2007). Widespread acceleration of tidewater glaciers on the Antarctic Peninsula. *Journal of Geophysical Research*, 112, F03S29. <https://doi.org/10.1029/2006JF000597>
- Raiswell, R. (2011). Iceberg-hosted nanoparticulate Fe in the Southern Ocean: Mineralogy, origin, dissolution kinetics and source of bioavailable Fe. *Deep-Sea Research Part II: Topical Studies in Oceanography*, 58, 1364–1375. <https://doi.org/10.1016/j.dsr2.2010.11.011>
- Reid, P., Stammerjohn, S., Masson, R. A., Barreira, S., Scambos, T., & Lieser, J. L. (2020). Sea ice extent, concentration, and seasonality (in “State of the Climate in 2019”). *Bulletin of the American Meteorological Society*, 101(8), S304–S306. <https://doi.org/10.1175/BAMS-D-20-0090.1>
- Saba, G. K., Fraser, W. R., Saba, V. S., Iannuzzi, R. A., Coleman, K. E., Doney, S. C., et al. (2014). Winter and spring controls on the summer food web of the coastal West Antarctic Peninsula. *Nature Communications*, 5, 4318. <https://doi.org/10.1038/ncomms5318>
- Scambos, T. A., Hulbe, C., Fahnestock, M., & Bohlander, J. (2000). The link between climate warming and break-up of ice shelves in the Antarctic Peninsula. *Journal of Glaciology*, 46, 516–530. <https://doi.org/10.3189/172756500781833043>
- Schofield, O., Saba, G., Coleman, K., Carvalho, F., Couto, N., Ducklow, H., et al. (2017). Decadal variability in coastal phytoplankton community composition in a changing West Antarctic Peninsula. *Deep-Sea Research Part I: Oceanographic Research Papers*, 124, 42–54. <https://doi.org/10.1016/j.dsr.2017.04.014>
- Sherman, J., Gorbunov, M. Y., Schofield, O., & Falkowski, P. G. (2020). Photosynthetic energy conversion efficiency in the West Antarctic Peninsula. *Limnology & Oceanography*, 65, 2912–2925. <https://doi.org/10.1002/lno.11562>
- Sherrell, R. M., Annett, A. L., Fitzsimmons, J. N., Rocanova, V. J., & Meredith, M. P. (2018). A ‘shallow bathtub ring’ of local sedimentary iron input maintains the Palmer Deep biological hotspot on the West Antarctic Peninsula shelf. *Philosophical Transactions of the Royal Society A*, 376(2122), 20170171. <https://doi.org/10.1098/rsta.2017.0171>
- Smale, D. A., Brown, K. M., Barnes, D. K. A., Fraser, K. P. P., & Clarke, A. (2008). Ice scour disturbance in Antarctic waters. *Science*, 321(5887), 371. <https://doi.org/10.1126/science.1158647>
- Smith, R. C., & Stammerjohn, S. E. (2001). Variations of surface air temperature and sea-ice extent in the western Antarctic Peninsula region. *Annals of Glaciology*, 33, 493–500. <https://doi.org/10.3189/172756401781818662>
- Smith, R. C., Stammerjohn, S. E., & Baker, K. S. (1996). Surface air temperature variations in the western Antarctic Peninsula region. In R. M. Ross, E. E. Hofmann, & L. B. Quetin (Eds.), *Foundations for ecological research west of the Antarctic Peninsula* (Vol. 70, pp. 105–121). American Geophysical Union. <https://doi.org/10.1029/ar070p0105>
- Spreen, G., Kaleschke, L., & Heygster, G. (2008). Sea ice remote sensing using AMSR-E 89-GHz channels. *Journal of Geophysical Research*, 113(C2), C02S03. <https://doi.org/10.1029/2005JC003384>
- Stammerjohn, S. E., Drinkwater, M. R., Smith, R. C., & Liu, X. (2003). Ice-atmosphere interactions during sea-ice advance and retreat in the western Antarctic Peninsula region. *Journal of Geophysical Research*, 108(C10). <https://doi.org/10.1029/2002JC001543>
- Stammerjohn, S. E., Martinson, D. G., Smith, R. C., & Iannuzzi, R. A. (2008). Sea ice in the western Antarctic Peninsula region: Spatio-temporal variability from ecological and climate change perspectives. *Deep-Sea Research Part II: Topical Studies in Oceanography*, 55, 2041–2058. <https://doi.org/10.1016/j.dsr2.2008.04.026>
- Stammerjohn, S. E., Martinson, D. G., Smith, R. C., Yuan, X., & Rind, D. (2008). Trends in Antarctic annual sea ice retreat and advance and their relation to El Niño–Southern Oscillation and Southern Annular Mode variability. *Journal of Geophysical Research*, 113, C03S90. <https://doi.org/10.1029/2007JC004269>
- Thomas, D. N., & Dieckmann, G. S. (2002). Antarctic sea ice—A habitat for extremophiles. *Science*, 295(5555), 641–644. <https://doi.org/10.1126/science.1063391>
- Thomas, E. R., Marshall, G. J., & McConnell, J. R. (2008). A doubling in snow accumulation in the western Antarctic Peninsula since 1850. *Geophysical Research Letters*, 35, L017606. <https://doi.org/10.1029/2007GL032529>

- Thompson, D. W. J., & Wallace, J. M. (2000). Annular modes in the extratropical circulation. Part I: Month-to-month variability. *Journal of Climate*, *13*, 1000–1016. [https://doi.org/10.1175/1520-0442\(2000\)013<1000:amitec>2.0.co;2](https://doi.org/10.1175/1520-0442(2000)013<1000:amitec>2.0.co;2)
- Thompson, D. W. J., Wallace, J. M., & Hegerl, G. C. (2000). Annular modes in the extratropical circulation. Part II: Trends. *Journal of Climate*, *13*, 1018–1036. [https://doi.org/10.1175/1520-0442\(2000\)013<1018:amitec>2.0.co;2](https://doi.org/10.1175/1520-0442(2000)013<1018:amitec>2.0.co;2)
- Tournadre, J., Bouhler, N., Girard-Ardhuin, F., & Rémy, F. (2016). Antarctic icebergs distributions 1992–2014. *Journal of Geophysical Research: Oceans*, *121*, 327–349. <https://doi.org/10.1002/2015JC011178>
- Tschudi, M. A., Meier, W. N., & Stewart, J. S. (2020). An enhancement to sea ice motion and age products at the National Snow and Ice Data Center (NSIDC). *The Cryosphere*, *14*(5), 1519–1536. <https://doi.org/10.5194/tc-14-1519-2020>
- Turner, J., Lu, H., White, I., King, J. C., Phillips, T., Hosking, J. S., et al. (2016). Absence of 21st century warming on Antarctic Peninsula consistent with natural variability. *Nature*, *535*(7612), 411–415. <https://doi.org/10.1038/nature18645>
- Turner, J., Maksym, T., Phillips, T., Marshall, G. J., & Meredith, M. P. (2013). The impact of changes in sea ice advance on the large winter warming on the western Antarctic Peninsula. *International Journal of Climatology*, *33*(4), 852–861. <https://doi.org/10.1002/joc.3474>
- Turner, J., Phillips, T., Marshall, G. J., Hosking, J. S., Pope, J. O., Bracegirdle, T. J., & Deb, P. (2017). Unprecedented springtime retreat of Antarctic sea ice in 2016. *Geophysical Research Letters*, *44*, 6868–6875. <https://doi.org/10.1002/2017GL073656>
- van den Broeke, M. R. (2005). Strong surface melting preceded collapse of Antarctic Peninsula ice shelf. *Geophysical Research Letters*, *32*, L12815. <https://doi.org/10.1029/2005GL025239>
- van Wessem, J. M., Meredith, M. P., Reijmer, C. H., van den Broeke, M. R., & Cook, A. J. (2017). Characteristics of the modelled meteoric freshwater budget of the western Antarctic Peninsula. *Deep-Sea Research Part II: Topical Studies in Oceanography*, *139*, 31–39. <https://doi.org/10.1016/j.dsr2.2016.11.001>
- van Wessem, J. M., van de Berg, W. J., Noël, B. P. Y., van Meijgaard, E., Amory, C., Birnbaum, G., et al. (2018). Modelling the climate and surface mass balance of polar ice sheets using RACMO2—Part 2: Antarctica (1979–2016). *The Cryosphere*, *12*(4), 1479–1498. <https://doi.org/10.5194/tc-12-1479-2018>
- Vaughan, D. G., Marshall, G. J., Connolley, W. M., Parkinson, C., Mulvaney, R., Hodgson, D. A., et al. (2003). Recent rapid regional climate warming on the Antarctic Peninsula. *Climatic Change*, *60*(3), 243–274. <https://doi.org/10.1023/a:1026021217991>
- Venables, H. J., Clarke, A., & Meredith, M. P. (2013). Wintertime controls on summer stratification and productivity at the western Antarctic Peninsula. *Limnology & Oceanography*, *58*(3), 1035–1047. <https://doi.org/10.4319/lo.2013.58.3.1035>
- Venables, H. J., & Meredith, M. P. (2014). Feedbacks between ice cover, ocean stratification, and heat content in Ryder Bay, western Antarctic Peninsula. *Journal of Geophysical Research: Oceans*, *119*(8), 5323–5336. <https://doi.org/10.1002/2013JC009669>
- Venables, H. J., Meredith, M. P., & Brearley, J. A. (2017). Modification of deep waters in Marguerite Bay, western Antarctic Peninsula, caused by topographic overflows. *Deep-Sea Research Part II: Topical Studies in Oceanography*, *139*, 9–17. <https://doi.org/10.1016/j.dsr2.2016.09.005>
- Vernet, M., Martinson, D., Iannuzzi, R., Stammerjohn, S., Kozłowski, W., Sines, K., et al. (2008). Primary production within the sea-ice zone west of the Antarctic Peninsula: I-Sea ice, summer mixed layer, and irradiance. *Deep-Sea Research Part II: Topical Studies in Oceanography*, *55*(18–19), 2068–2085. <https://doi.org/10.1016/j.dsr2.2008.05.021>
- Wallace, M. I., Meredith, M. P., Brandon, M. A., Sherwin, T. J., Dale, A., & Clarke, A. (2008). On the characteristics of internal tides and coastal upwelling behavior in Marguerite Bay, west Antarctic Peninsula. *Deep-Sea Research Part II: Topical Studies in Oceanography*, *55*(18–19), 2023–2040. <https://doi.org/10.1016/j.dsr2.2008.04.033>